https://doi.org/10.5194/egusphere-2022-1365
Preprint. Discussion started: 2 January 2023

The impact of rotational rifting on the evolution of the East African Rift System: an analogue modelling study

Frank Zwaan[1,2], Guido Schreurs[1]

[1]Institute of Geological Sciences, University of Bern, Baltzerstasse 1+3, 3012 Bern, Switzerland
[2]Helmholtz Centre Potsdam - GFZ German Research Centre for Geosciences, Potsdam, Germany

Correspondence to: Frank Zwaan (frank.zwaan@gfz-potsdam.de)

Keywords: East African Rift, Nubian Plate, Somalia Plate, Victoria Plate, rifting, rotational extension, continental breakup, analogue modelling, monitoring techniques

Short Summary: The East African Rift System (EARS) is a major plate tectonic feature splitting the African continent apart. Understanding the tectonic processes involved is of great importance for societal and economic reasons (natural hazards, resources). Laboratory experiments allow us to simulate these large-scale processes, highlighting the impact of rotational plate motion on the overall development of the EARS, an insight relevant to our interpretation of other rift systems around the globe as well.

Abstract: The East African Rift System (EARS) represents a major tectonic feature splitting the African continent apart into the Nubian Plate situated to the west, and the Somalian Plate to the east. The EARS comprises various rift segments and two microplates (the Victoria and Rovuma plates) and represents a key location for studying rift evolution. Researchers have proposed various scenarios for the evolution of the EARS, but the impact of continental-scale rotational rifting, caused by the rotation of the Somalian Plate, has received only limited attention. In this study we apply analogue models to explore the dynamic evolution of the EARS within the broader rotational rifting framework. Our models show that rotational rifting leads to the lateral propagation of deformation towards the rotation axis, but we must distinguish between the propagation of distributed deformation, which can move very rapidly, and localized deformation, which can significantly lag behind. The various structural weakness arrangements in our models (representing pre-existing structural heterogeneities) lead to a variety of different structures. Laterally overlapping weaknesses are required for localizing parallel rift basins to create rift pass structures, possibly leading to the rotation and segregation of micro-plates, as is the case for the Victoria Plate in the EARS. Additional model observations concern the development of early pairs of rift-bounding faults flanking the rift basins, followed by the localization of deformation along the axes of the most advanced rift basins. Furthermore, the orientation of rift segments with respect to the regional (rotational) plate divergence affects deformation along these segments: oblique rift segments are less wide due to a strike-slip deformation component. Overall, our model results are a good fit with the large-scale features of the EARS, providing constraints on the timing of rift development and on the segregation and rotation of the Victoria plate within the broader rotational rifting framework of the EARS.

https://doi.org/10.5194/egusphere-2022-1365
Preprint. Discussion started: 2 January 2023

1. Introduction

The East African Rift System (EARS) represents a major tectonic feature that splits the African continent in two main plates: the Nubian Plate situated to the west, and the Somalian Plate to the east (e.g., Morley et al., 1999; Chorowicz, 2005; Ring, 2014; Macgregor, 2015; Fig. 1a, b). From its northern end in the Afar triangle, where the rift merges with the Red Sea and Gulf of Aden basins, the EARS stretches some 5000 km southward, comprising various rift segments and branches, including two microplates (the Victoria and Rovuma plates) (Ebinger, 1989; Chorowicz, 2005; Corti, 2012; Michon et al., 2022, Fig. 1a, b). The EARS is a key location for the study of rift evolution as it contains rift basins in various stages of development, from young continental rift basins to incipient continental break-up situations (e.g., Chorowicz, 2005; Ebinger, 2005; Corti, 2012, Fig. 1a, b).

Researchers have proposed various scenarios for the development of the EARS, based on a variety of observations (see discussion in Morley, 2010 and Glerum et al., 2020, Fig. 1b-d). The first general scenario involves a large-scale NW-SE plate divergence causing rifting along the various rift segments, with offsets between the segments accommodated by large-scale NW-SE oriented strike-slip zones (e.g., Wheeler and Karson, 1994; Scott et al., 1989; Chorowicz, 2005). For the second scenario a general E-W plate divergence is proposed, where the type of faulting along the rift segments (pure normal faulting or [partial] strike-slip faulting) is controlled by the orientation of pre-existing weaknesses (e.g., Ebinger, 1989; Lezzar et al. 2002). A variant of this second scenario invokes dominant normal faulting due to local rift segment-orthogonal extension resulting from stress-deflection along the various branches of the EARS (Morley 2010; Delvaux et al. 2012). Recently, Glerum et al. (2020) have shown through numerical modelling efforts that the various observations on which these competing scenarios are based can be reconciled in a model involving general E-W plate divergence, where the overlapping branches of the EARS (i.e. the Western Rift/Branch and the Eastern Branch/Kenya Rift) that are localized along inherited weaknesses cause the Victoria Plate between them to rotate in a counter-clockwise fashion (a so-called “rift pass” structure, e.g. Oldenburg and Brune, 1975; Nelson et al., 1992; Hieronymus, 2004; Katz et al., 2005; Tentler and Accocella, 2010; Brune et al., 2017; Zwaan et al., 2018a, Fig. 1c).

However, Glerum et al. (2020) did not incorporate the rotational motion of the Somalian Plate, which causes a gradual southward decrease in plate divergence velocity (Saria et al., 2014; Stamps et al., 2014, 2021 Fig. 1a), into their models. Various tectonic modelling studies have shown that such plate divergence gradients have important effects on the evolution of rift systems (e.g. Souriot and Brun, 1992; Benes and Scott, 1996; Sun et al., 2009; Molnar et al., 2017, 2018; Zwaan et al., 2020; Schmid et al., 2022a). In a recent study, Zwaan and Schreurs (2020) presented a first-order modelling study exploring the rift interaction structures in rotational and orthogonal rifting settings (Fig. 1d) Their results suggested that rotational rifting should indeed have an effect on the evolution of the EARS, explaining the large-scale southward younging trend of the rift system as reported by e.g. Chorowicz (2005) and Macgregor (2015). However, these were generic models, focussed on

https://doi.org/10.5194/egusphere-2022-1365
Preprint. Discussion started: 2 January 2023

systematically testing the effects of simple initial rift arrangement, so that the comparison with the EARS as presented by Zwaan and Schreurs (2020) remains rather coarse (Fig. 1d).

Hence we here present a new series of rotational rifting models specifically tailored to the tectonic situation in the EARS, with the aim to explore the dynamic evolution of the rift system in more detail. We find that our models provide a good fit with the large-scale features of the EARS, and provide constraints on the timing of general rift development, and the segregation and rotation of the Victoria plate within the broader rotational rifting framework of the EARS.

https://doi.org/10.5194/egusphere-2022-1365
Preprint. Discussion started: 2 January 2023

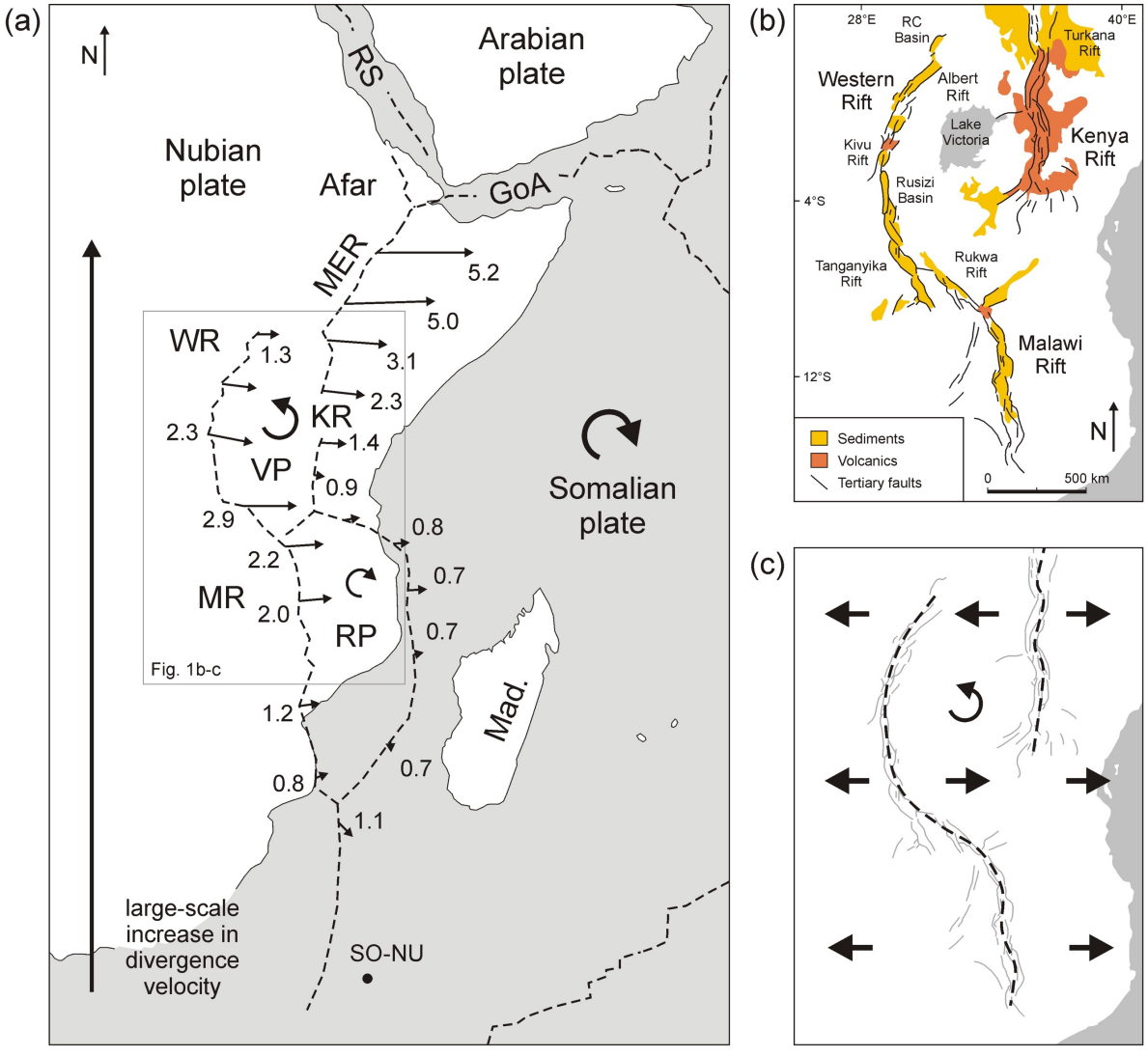

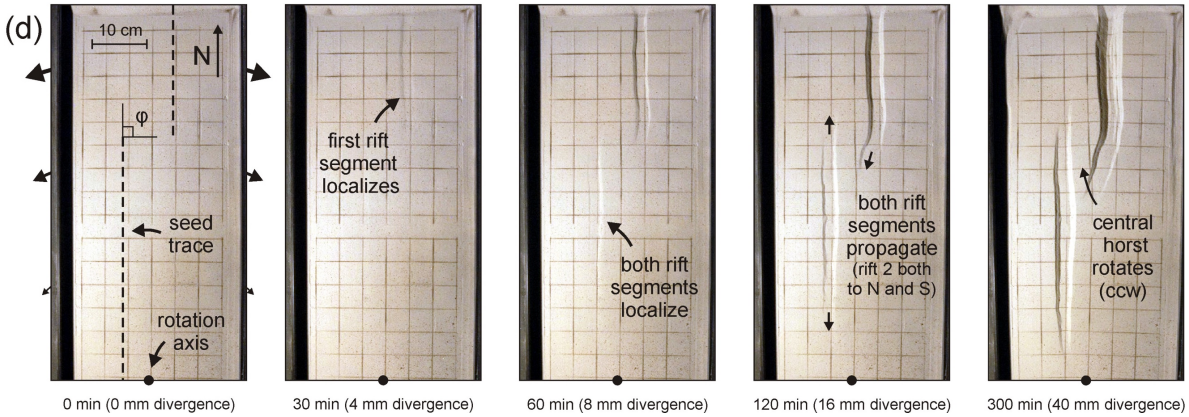

https://doi.org/10.5194/egusphere-2022-1365
Preprint. Discussion started: 2 January 2023

Figure. 1: (a) Tectonic outline of the East African Rift System (EARS) showing the rotation of the Somalian Plate, the Victoria plate (VP) and the Rovuma Plate (RP). Plate motions (in mm/yr), modified after Saria et al. (2014). GoA: Gulf of Aden, KR: Kenya Rift, MER: Main Ethiopian Rift, MR: Malawi Rift, RP: Rovuma Plate, RC: Rhino-Camp, RS: Red Sea, SO-NU: Somalia Nubia rotation pole, WR: Western Rift. (b) detailed structural map of the EARS. Modified after Ebinger (1989). (c). Tectonic models proposed for the EARS, after Glerum et al. (2020). (d) Analogue models of rift interaction in a rotational rifting setting by Zwaan and Schreurs (2020). ccw: counterclockwise, φ: angle between the seed (i.e. inherited weakness) orientation and the line between both seed tips (90˚ in this case, i.e. no lateral seed overlap),

2. Methods

2.1. Set-up

We apply a rotational extension set-up with a brittle-viscous layering, based on previous modelling efforts by Zwaan and Schreurs (2020), Zwaan et al. (2020), and Schmid et al. (2022a, b) (Fig. 1). Prior to model preparation, an 8 cm thick foam block (RG 50 polyurethane foam base from GOBAG, www.gobag.ch) is compressed between two longitudinal sidewalls, on which the brittle-viscous model materials (1.5 cm quartz sand on top of a 3 cm thick viscous mixture representing a 150 km thick lithosphere and the upper 300 km of the sub-lithospheric mantle) are applied. One of the sidewalls is mobile and connected to a rotation axis, allowing it to rotate in a clockwise fashion, thus simulating the rotation of the Somalian Plate with respect to the Nubian Plate (Fig. 1). During this rotational motion of the mobile sidewall at a rate of 4 mm/h at the farthest point from the rotation axis, the foam base expands, inducing extension in the overlying model materials with a southwardly decreasing gradient (Fig. 2c, d). Given the model duration of 150 min, the total extension is 10 mm at the farthest point from the rotation axis.

In order to localize deformation, we include seeds that follow (parts of) the trace of the rift basins that comprise the EARS (Fig. 2a-c, e). These seeds are thin (ø 4 mm) thick semi-cylindrical bars of viscous material applied on top of the basal viscous layer, causing the overlying sand layer to be locally thinned and weakened (Fig. 2b). Such seeds tend to produce strongly localized rift basins and are deemed ideal to reproduce the localized style of deformation along the EARS. We tested five main combinations of seed geometries, as depicted in Fig 2e, where the seed representing the Western Rift in Model D (Fig. 1, 2e) has a double thickness of 8 mm. The summarized results of one further experiment are presented in the Appendix. Detailed results regarding all models included in this paper are provided in the supplementary material (Zwaan and Schreurs, 2023).

https://doi.org/10.5194/egusphere-2022-1365
Preprint. Discussion started: 2 January 2023

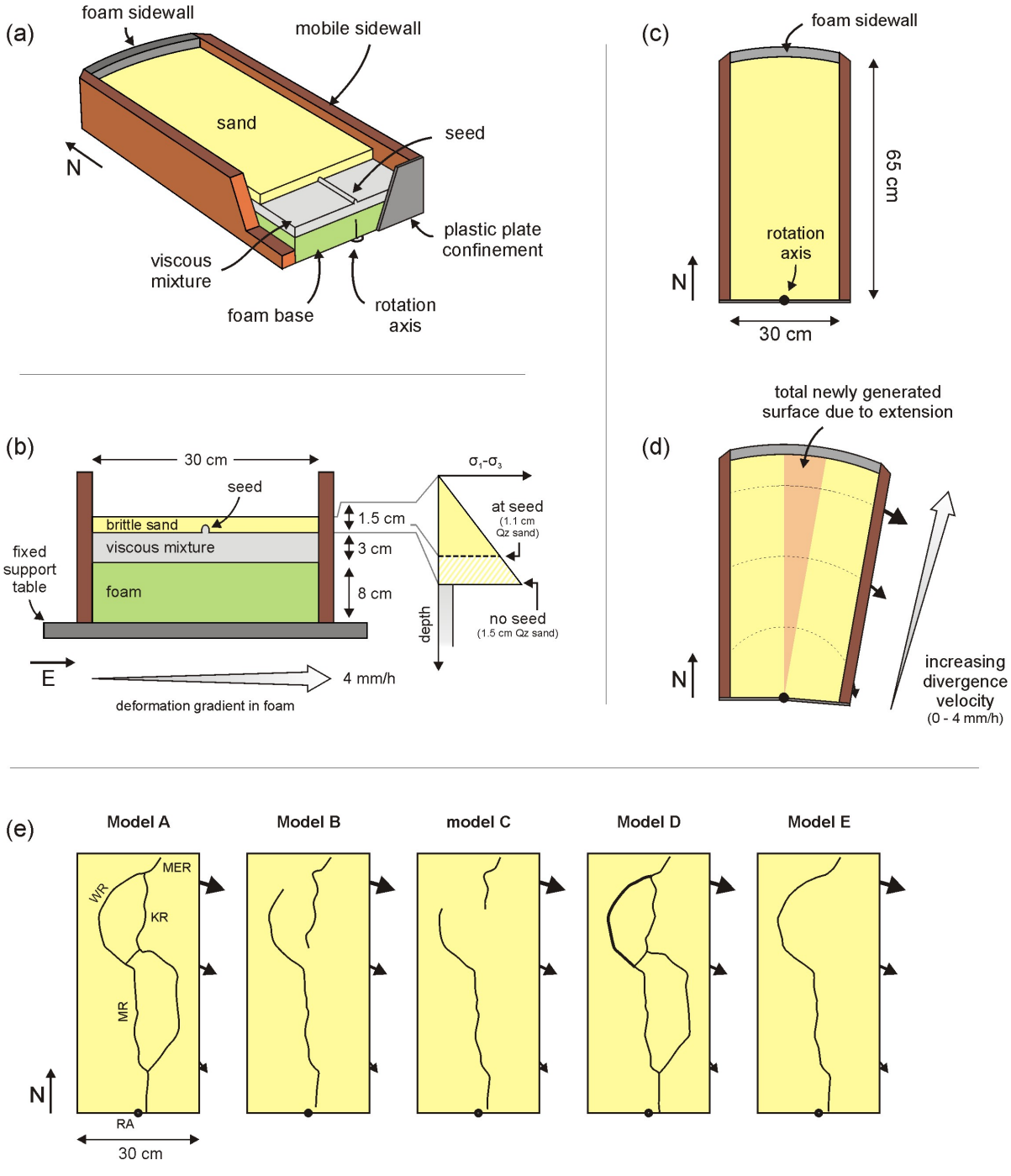

Figure 2: Model setup. (a) 3D sketch of model set-up. (b) cross-section of model set-up. (c) top view of model set-up prior to deformation, and (d) after rotational deformation. (e) Seed geometries applied for Models A-E, where Model D contains a double thickness seed along the simulated Western Rift (WR). The seed geometries are based on the rift arrangement in the East African Rift System (EARS), as presented in Fig. 1a and indicated in the panel of Model A. KR: Kenya Rift, MER: Main Etiopian Rift, MR: Malawi Rift. Note that the rotation axis (RA) is situated somewhat too much to the west when compared to the natural case (Fig. 1a), but this does not affect the model results in any significant fashion (see description of Model F in the Appendix).

https://doi.org/10.5194/egusphere-2022-1365
Preprint. Discussion started: 2 January 2023

2.2. Materials

We use a brittle-viscous model layering with a 1.5 cm thick top layer consisting of quartz sand representing a 150 km lithosphere dominated by brittle deformation (1 cm = 100 km). This quartz sand (Quarzsand A from Carlo Bernasconi AG, www.carloag.ch) has a grain size of 60-250 µm and internal friction angles between 31.4˚-36.1˚, with a cohesion value of 9 Pa (Zwaan et al., 2018b) (Table 1). The sand has a constant density of 1560 kg/m^3 when sieved from ca. 30 cm height (Schmid et al., 2020), and is flattened by a scraper at the end of deformation to ensure a flat model surface.

The underlying 3 cm thick viscous layer representing the sub-lithospheric mantle consists of a near-Newtonian mixture of SGM-36 Polydimethyl-siloxane (PDMS) and corundum sand (F120 Edelkorund) from Carlo AG (η = ca. 1.5·105 Pa·s; n = 1.05-1.10, Zwaan et al., 2018c). The materials are mixed following a 0.965 : 1.00 weight ratio and the density of the resulting viscous mixture is similar to that of the sand layer (ca. 1600 kg/m3). Further material properties are presented in Table 1.

Table 1: Model materials

Granular materials	**Quartz sand[a]**	**Corundum sand[b]**
Grain size range	60-250 µm	88-125 µm
Density (bulk material)[c]	2650 kg/m^3	3950 kg/m^3
Density (sieved)	1560 kg/m^3	1890 kg/m^3
Angle of internal peak friction	36.1˚	37˚
Angle of dynamic-stable friction	31.4˚	32˚
Angle of reactivation friction	33.5˚	-
Cohesion	9 ± 98 Pa	39 ± 10 Pa
Viscous materials	**Pure PDMS[a, d]**	**PDMS / corundum sand mixture[a]**
Weight ratio PDMS / corundum sand	-	0.965 kg / 1.00 kg
Density	965 kg/m^3	1600 kg/m^3
Viscosity	ca. 2.8·10^4 Pa·s	ca. 1.5·10^5 Pa·s[e]
Rheology[f]	Newtonian (n = 1)	near-Newtonian (n = 1.05-1.10)

[a] Quartz sand, PDMS and viscous mixture characteristics after Zwaan et al. (2016, 2018b, c)
[b] Corundum sand characteristics after Panien et al. (2006)
[c] Specific densities after Carlo AG (2022)
[d] Pure PDMS rheology after Rudolf et al. (2016)
[e] Viscosity value holds for model strain rates < 10^{-4} s^{-1}
[f] Power-law exponent *n* (dimensionless) represents sensitivity to strain rate

https://doi.org/10.5194/egusphere-2022-1365
Preprint. Discussion started: 2 January 2023

2.3. Scaling

We use standard scaling methods to make sure our analogue models adequately represent the natural situation in the EARS (see scaling values in Table 2). Since brittle materials have strain rate-independent rheologies, the angle of internal friction of our quartz sand is the main factor for scaling purposes. Since (36.1°) is very similar to values found in (upper crustal) rocks (31-38°, Byerlee, 1978, Table 2), our quartz sand is appropriate to represent the lithosphere in our models.

Scaling viscous materials becomes more intricate than scaling brittle materials due to the strain rate-dependent rheology of the former. Using the stress ratio between model and nature (σ^*, convention: $\sigma^* = \sigma_{model}/\sigma_{nature}$): $\sigma^* = \rho^* \cdot h^* \cdot g^*$, where ρ^*, h^* and g^* are density, length and gravity ratios, respectively (Hubbert, 1937; Ramberg, 1981) and the viscosity ratio (η^*), we obtain the strain rate ratio ε^* (Weijermars and Schmeling 1986): $\dot{\varepsilon}^* = \sigma^*/\eta^*$. With the strain rate ratio we can subsequently compute the velocity and time ratios (v^* and t^*): $\dot{\varepsilon}^* = v^*/h^* = l/t^*$. Given a viscosity of $1 \cdot 10^{20}$ Pa·s for the sub-lithospheric mantle, our 4 mm/h divergence velocity scales up to ca. $1 \cdot 10^5$ mm/yr. Although this velocity is much higher than typical rift divergence rates along the EARS (e.g., Saria et al., 2014, Fig. 1), we do not consider this to be a major issue here. Previous modelling efforts have shown that high extension rates can lead to increased brittle-viscous coupling and distributed extension or "wide rifting" (e.g. Brun, 1999; Zwaan et al., 2016, 2019). However, as long as the seeds localize deformation properly, and no indications of distributed rifting are observed (as is clearly the case in our models), the high divergence velocity in our models can be deemed acceptable.

In addition, we consider the dynamic similarity of the model to the natural example through the Rs ratio and the Ramberg number. We derive the dynamic similarity between the brittle sand layer and the natural lithosphere using the Rs ratio between the gravitational stress and the cohesive strength or cohesion C (Ramberg, 1981; Mulugeta, 1988): R_s = gravitational stress/cohesive strength = $(\rho \cdot g \cdot h)/C$. When assuming a combined cohesion of 100 MPa for the lithosphere, together with the 9 Pa cohesion of our quartz sand, we obtain a R_s of 26 for our models and 27 for the natural example. The Ramberg number R_m considers the dynamic similarity scaling of viscous materials (Weijermars and Schmeling 1986): R_m = gravitational stress/viscous strength = $(\rho \cdot g \cdot h^2)/(\eta \cdot v)$, and has a value of 85 for both the viscous mixture and the sub-lithospheric mantle in nature, respectively. Since both the R_s and R_m values of our models are quite similar to those in their natural equivalent, we considered our models sufficiently adequately scaled for simulating large-scale continental rifting processes.

https://doi.org/10.5194/egusphere-2022-1365
Preprint. Discussion started: 2 January 2023

Table 2: Scaling parameters

		Model	Nature
General parameters	Gravitational acceleration (g)	9.81 m/s^2	9.81 m/s^2
	Divergence velocity (v)	1.1·10^{-6} m/s*	3.4·10^{-7} m/s
Brittle layer	Material	Quartz sand	Lithosphere
	Peak internal friction angle (φ)	36.1°	30-38°
	Thickness (h)	1.5·10^{-2} m	1.5·10^5 m
	Density (ρ)	1560 kg/m^3	2800 kg/m^3
	Cohesion (C)	9 Pa	1.5·10^8 Pa
Viscous/ ductile layer	Material	PDMS/corundum sand mixture	Sub-lithospheric mantle
	Thickness (h)	3·10^{-2} m	3·10^5 m
	Density (ρ)	1600 kg/m^3	3300 kg/m^3
	Viscosity (η)	1.5·10^5 Pa·s	1·10^{20} Pa·s
Dynamic scaling values	Brittle stress ratio (R_s)	26	27
	Ramberg number (R_m)	85	85

* maximum divergence velocity, away from the rotation axis

2.4. Model monitoring and analysis

We monitor the surface evolution of our models through time-lapse photography, by means of a camera set-up consisting of 3 (obliquely oriented) high-resolution Nikon D810 (36.3 MP) cameras (Zwaan et al. 2021, 2022; Schmid et al. 2022a, b). Map view images together with a 4 x 4 cm surface grid made of corundum sand (<1 mm thick) provides a first-order insight into model evolution). Additional model surface analysis involves photogrammetry on time-lapse imagery from the (obliquely oriented) cameras with Agisoft Photoscan software, www.agisoft.com) to generate digital elevation models, enabling an assessment of model topography variations over time, notably rift basin evolution, by means of GIS software (e.g. QGIS, www.qgis.org), (Fig. 4b). The time-lapse imagery also allows a more detailed analysis and quantification of model surface deformation through means of digital image correlation (DIC) techniques (e.g. Adam et al., 2005, Boutelier et al. 2019, and references therein). This DIC analysis involves the tracing of horizontal displacements between different time steps (here 10

https://doi.org/10.5194/egusphere-2022-1365
Preprint. Discussion started: 2 January 2023

mm of divergence) using LaVision DaVis 10.2 DIC software. From the horizontal displacement data we derive incremental and cumulative maximum normal strain maps that serve as a proxy for tracing active deformation in the models over time.

3. Results

3.1. Model A

The results of Model A, with standard thickness seeds (ø 4 mm) tracing all EARS plate boundaries, are presented in Fig. 3. Topography data show that early deformation is not clearly expressed compared to what is revealed in the DIC results. The first hints of topographic deformation appear in the northernmost part of the model after some 20 to 30 minutes, at the simulated Main Ethiopian Rift – Kenya rift location (Fig 3b, c). Subsequently a mostly N-S oriented through-going rift system develops as rift-related subsidence propagates southward, crossing over into the simulated Malawi Rift. Minor subsidence is visible at the simulated Western Rift as well, but there is no trace of deformation west of the simulated Rovuma Plate (Fig. 3).

In contrast to the topography data, the DIC results show that deformation was in fact already localizing during the earliest stages of the model run (Fig. 3g, m). After 10 minutes, extensional deformation was developing along large parts of the most central seed segments. These structures develop conjugate sets of rift boundary faults as indicated by the parallel bands of localized deformation, and all structures active in Model A are seen to be deforming by the 20 minute mark (Fig. 3h, n) when the simulated Western Rift is also being active to a moderate degree, the effect of which is also nicely visible in the eastward displacement results (Fig. 3n, o). Furthermore, the clear northward increase in eastward displacement seen in the eastern part of the model highlights the clockwise rotational motion applied to the system (Fig. 3m-r). Note also the much less expressed gradient on the western side of the model, indicating some minor rotation there as well, which we regard to be a boundary effect (Fig. 3m-r).

Some additional important details are revealed by the DIC results. Firstly, we find that the southward propagation of active deformation is indeed largely completed after 20 minutes, but it continues at a slow rate until the end of the model run (Fig. 3g-l). Furthermore, towards the end of the model run, the most advanced rift basins in the model (the simulated Kenya and Malawi rifts) seem to develop a central band of extensional deformation in addition to the active rift boundary faults (Fig. 3l).

https://doi.org/10.5194/egusphere-2022-1365
Preprint. Discussion started: 2 January 2023

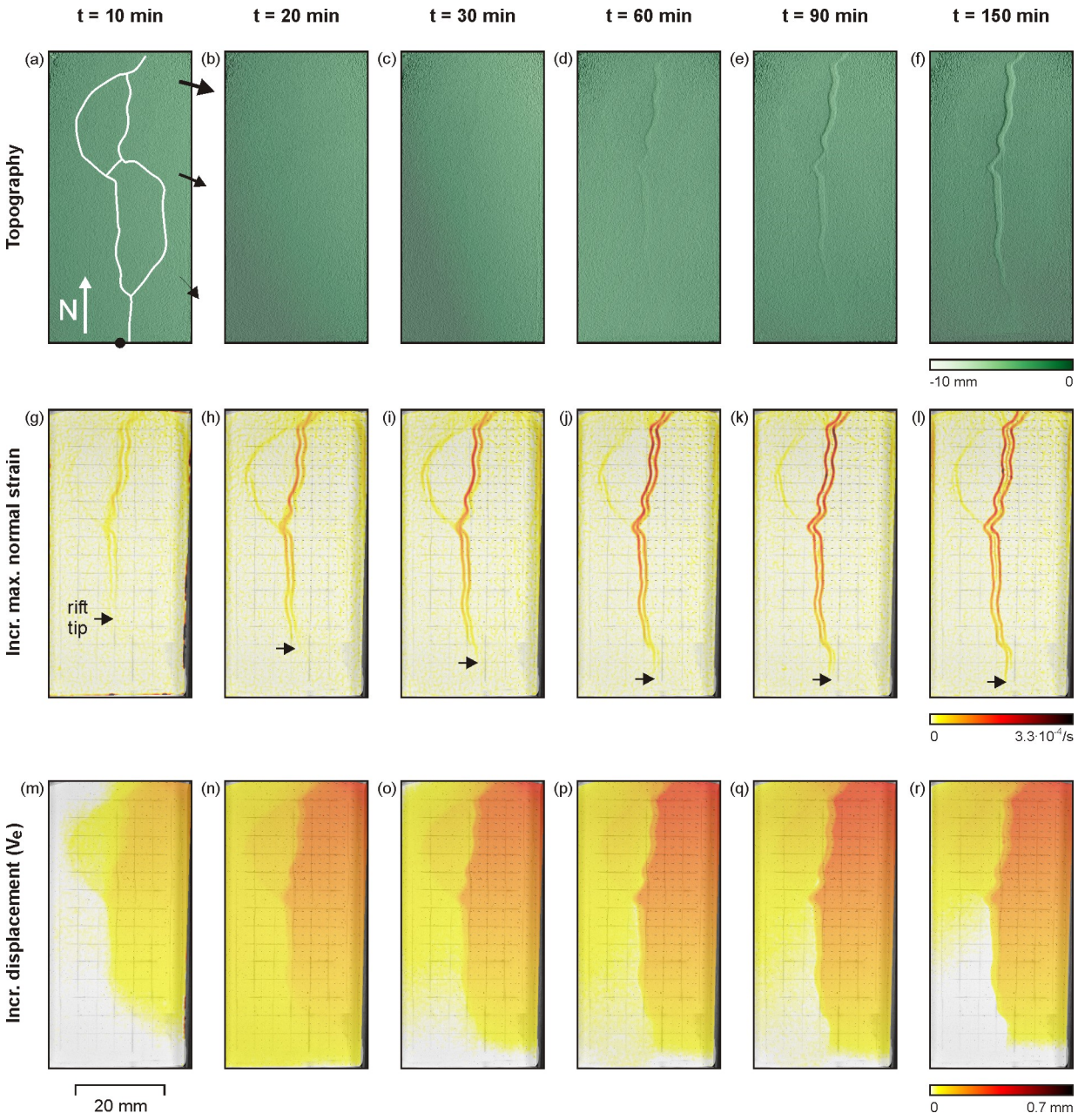

Figure 3: Results of Model A. (a-f) Topography evolution. Initial seed geometry is shown in panel (a). Lighting direction: from the left. (g-l) Incremental maximum normal strain (m-r). Incremental eastward displacement (Ve). Increments for digital image correlation (DIC) analysis: 10 minutes of divergence.

https://doi.org/10.5194/egusphere-2022-1365
Preprint. Discussion started: 2 January 2023

3.2. Model B

Model B, has the same standard thickness seeds as Model B (ø 4 mm), but the seeds trace less of the EARS plate boundaries (Fig. 4). The topography evolution results are similar to those in Model A, in that they reveal the earliest rift development around the 20/30-minute mark (Fig. 4b), and some general propagation of rift-related subsidence over time. However, a major difference is that in this model, the simulated Western Rift is much better developed, and there is only a minor connection between the simulated Rukwa Rift between the Kenya Rift and Malawi Rift, whereas Model A features a through-going rift basin.

The DIC results provide important additional details (Fig. 4g-r). As in Model A, deformation already localizes in the early stages, before it becomes visible at the model surface. We also observe that most structures are already activated around t = 20 min. The main differences with Model A are related to the increased development of the simulated Western Rift, as highlighted by the eastward displacement analysis (Fig. 4m-r). This analysis shows the same general rotation imposed along the eastern bound of the model, but the simulated Western Rift's development causes the presence of the Victoria Plate equivalent, which undergoes a counter-clockwise rotation (as indicated by the decreasing eastward displacement towards the north, Fig. 4m-r).

Further important details are that similar to Model A, we observe a relatively fast early southward propagation of active extension followed by slow propagation during the rest of the model run (Fig. 3g-l), and intra-rift deformation along the most developed rift basin (the simulated Kenya Rift, Fig. 3l). An additional observation from DIC data is that the simulated Western Rift initiates its development in the south, and gradually propagates northward, eventually deflecting northward (Fig. 4g-l). Finally, both the DIC and topography data show that the link between the simulated Western Rift and Malawi rift, which is 45˚ oblique to the model axis, is rather narrow compared to those rift segments that are more parallel to the model axis (Fig. 4g-r).

https://doi.org/10.5194/egusphere-2022-1365
Preprint. Discussion started: 2 January 2023

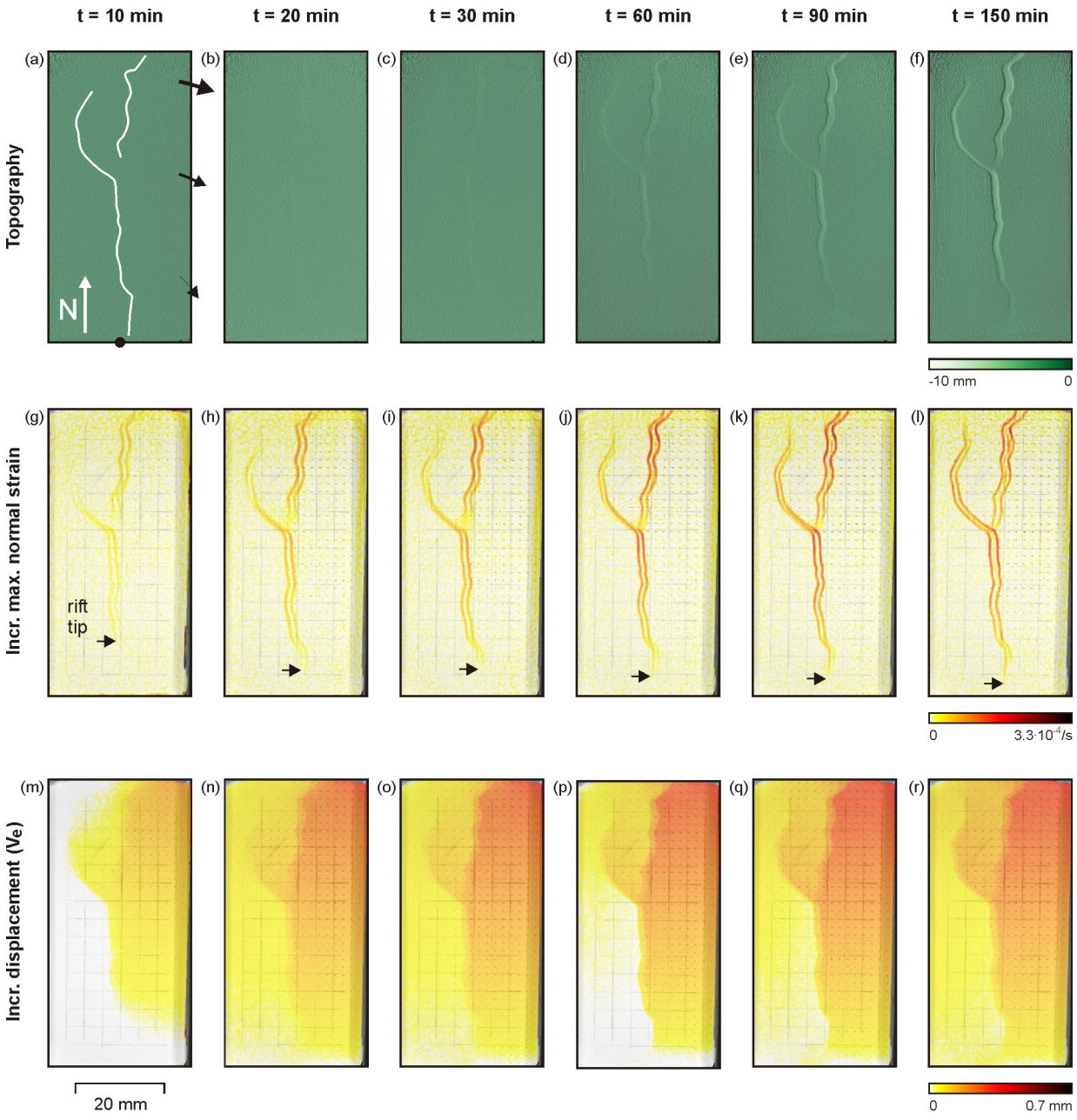

Figure 4: Results of Model B. (a-f) Topography evolution. Initial seed geometry is shown in panel (a). Lighting direction: from the left. (g-l) Incremental maximum normal strain (m-r). Incremental eastward displacement (Ve). Increments for digital image correlation (DIC) analysis: 10 minutes of divergence.

https://doi.org/10.5194/egusphere-2022-1365
Preprint. Discussion started: 2 January 2023

3.3. Model C

Model C is a rerun of Model B, with a slightly reduced seed length in both the simulated Kenya and Western rifts, so that the seeds do not laterally overlap (similar to the models from Zwaan et al. 2020, Figs. 1d, 5a). The result is fairly similar to Model B (Fig. 4), with the earliest signs of deformation from topography data occurring after 20-30 minutes, whereas DIC results reveal active extension throughout large parts of the model at the 10-minute mark (Fig. 5b, c, g). However, the reduced seed presence reduces the topographical impact of the simulated Kenya and Western Rifts, even though DIC results show (distributed) extension past the rift tips (Fig. 5f, l). Note that the simulated Western Rift does not deflect as far northward as in Model B, but does generally propagate northward along the trace of the seed, and as a result of its activity the counter-clockwise rotating Victoria equivalent is established (Fig. 5g-r). Parallel to its Western Rift equivalent, the simulated Kenya Rift propagates southward, but the southern rift tip ends in a diffuse zone (Fig. 5g-l). Similar to Models A and B, southward propagation of extension is observed, decelerating after 20 minutes but never fully halting (Fig. 5g-l), and intra-rift deformation is localizing along the axes of the most developed rift segments (Kenya and Malawi Rifts, Fig. 5l). Furthermore, as seen in Model B, the ca. 45˚ oblique link Rukwa Rift is rather narrow compared to other, less obliquely oriented, rift segments (Fig. 5f, l).

3.4. Model D

Model D is a rerun of Model A, with a double thickness seed (ø 8 mm) tracing the Western Rift (Figs. 2e, 6). Also in this model, topography data indicates the first signs of deformation around the 20/30-minute mark (Fig. 6b, c), whereas DIC results clearly show that extension is already localizing at t = 10 min (Fig. 6g). In contrast to Model A, however, the dominant rift branch in the north of the model is the simulated Western Rift (instead of the Kenya Rift) (Fig 6f, l). Hence we obtain a largely westwardly curved rift system in the north of the model, with only minor deformation at the simulated Kenya Rift (Fig. 6f, l). As a result of this configuration, all domains east of the dominant Western Rift equivalent are moving eastward, where the simulated Kenya Rift slightly mitigates this effect so that a generally eastward moving Victoria Plate equivalent can be observed (Fig. 6m-r). Note that in contrast to Models B and C, this microplate does not rotate as indicated by the lack of a clear displacement gradient (Figs. 4m-r, 5m-r, 6m-r).

Also in this model, we see that the general southward propagation of extension is strongly decelerating after 20 min, but no northward propagation is seen in the simulated Western Rift (Fig. 6g-l). Furthermore, not only is the oblique link Rukwa Rift segment between the simulated Western Rift and Malawi Rift narrower in shape than the ca. N-S oriented rift basins, this is also true of the highly oblique link between the simulated Western Rift and the Main Ethiopian Rift in the north (Fig. 6f, l). Finally, although it is not that clear, there are some hints of intra-rift deformation in the simulated Malawi Rift, Western Rift, and Main Ethiopian Rift (Fig. 6l).

https://doi.org/10.5194/egusphere-2022-1365
Preprint. Discussion started: 2 January 2023

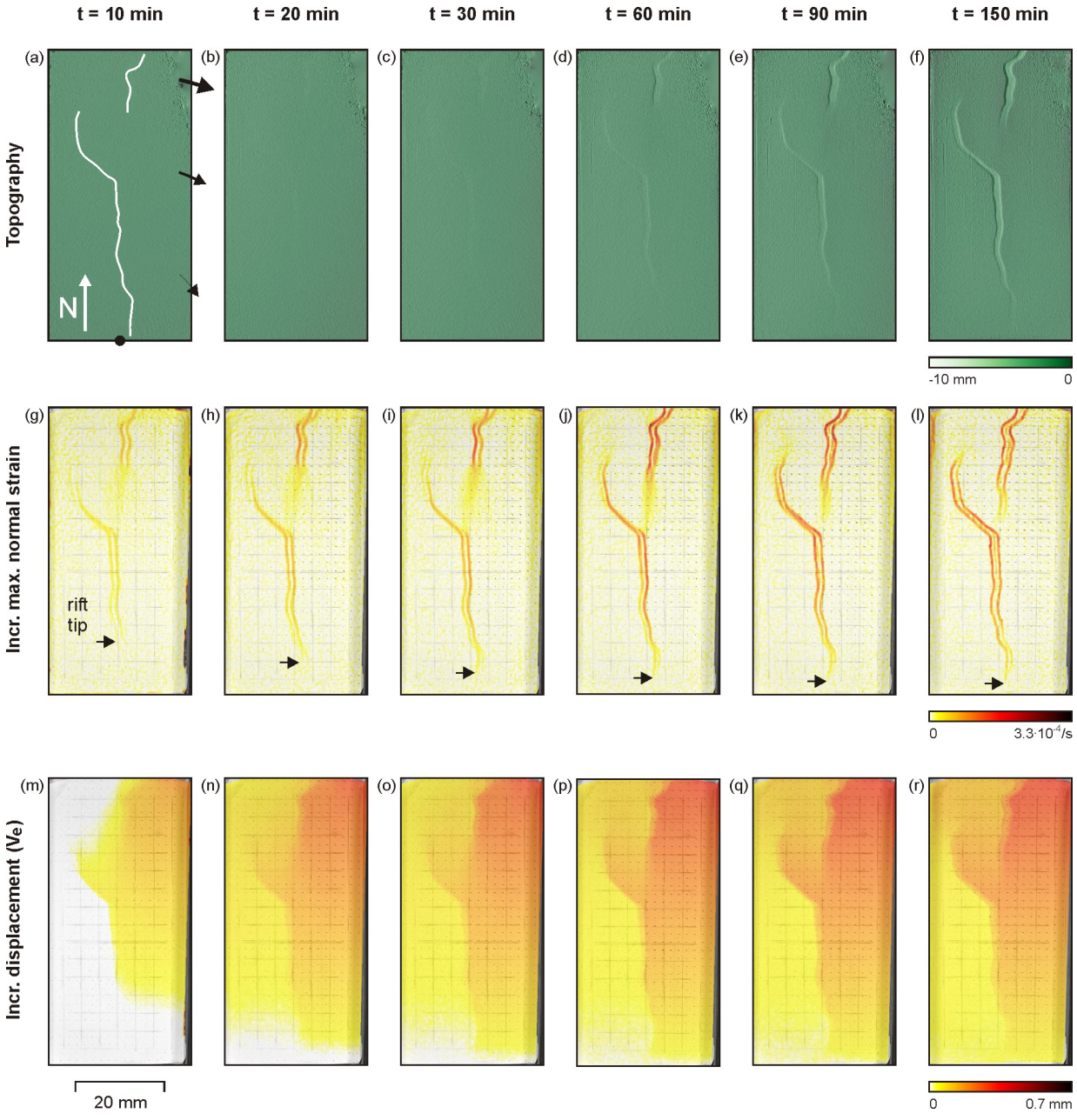

Figure 5: Results of Model C. (a-f) Topography evolution. Initial seed geometry is shown in panel (a). Lighting direction: from the left. (g-l) Incremental maximum normal strain (m-r). Incremental eastward displacement (Ve). Increments for digital image correlation (DIC) analysis: 10 minutes of divergence.

https://doi.org/10.5194/egusphere-2022-1365
Preprint. Discussion started: 2 January 2023

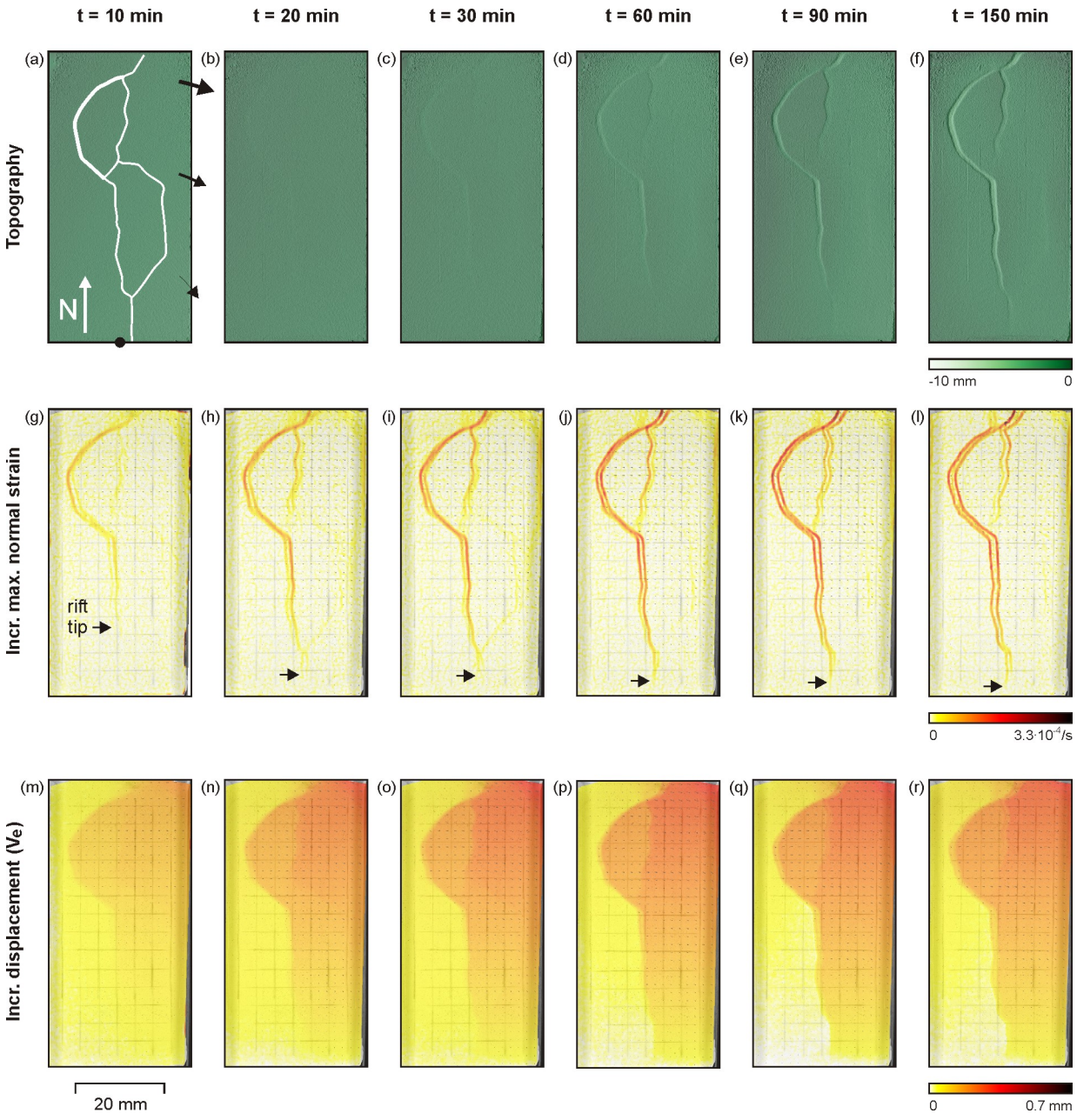

Figure 6: Results of Model D. (a-f) Topography evolution. Initial seed geometry is shown in panel (a), where the Western Rift seed had a double diameter (ø 8 mm). Lighting direction: from the left. (g-l) Incremental maximum normal strain (m-r). Incremental eastward displacement (Ve). Increments for digital image correlation (DIC) analysis: 10 minutes of divergence.

https://doi.org/10.5194/egusphere-2022-1365
Preprint. Discussion started: 2 January 2023

3.5. Model E

In Model E, we apply a standard thickness seed that follows the westernmost limits of the EARS (Fig. 7a). The results are very similar to those of Model D, even though the seed geometry is quite different (Figs. 6, 7). We observe the development of a rift system along the length of the seed, following the various curves of said seed. After 20/30 minutes the earliest structures become visible at the surface (Fig. 7b, c), whereas DIC analysis shows early extension along most of the seed, which propagates southward until the 20 minute mark, before slowing down drastically (Fig. 7g-l). Similar to the structures in Model D, the oblique parts of the rift system are narrower, and all domains east of the rift system move eastward (Fig. 7f, l, m-r).

https://doi.org/10.5194/egusphere-2022-1365
Preprint. Discussion started: 2 January 2023

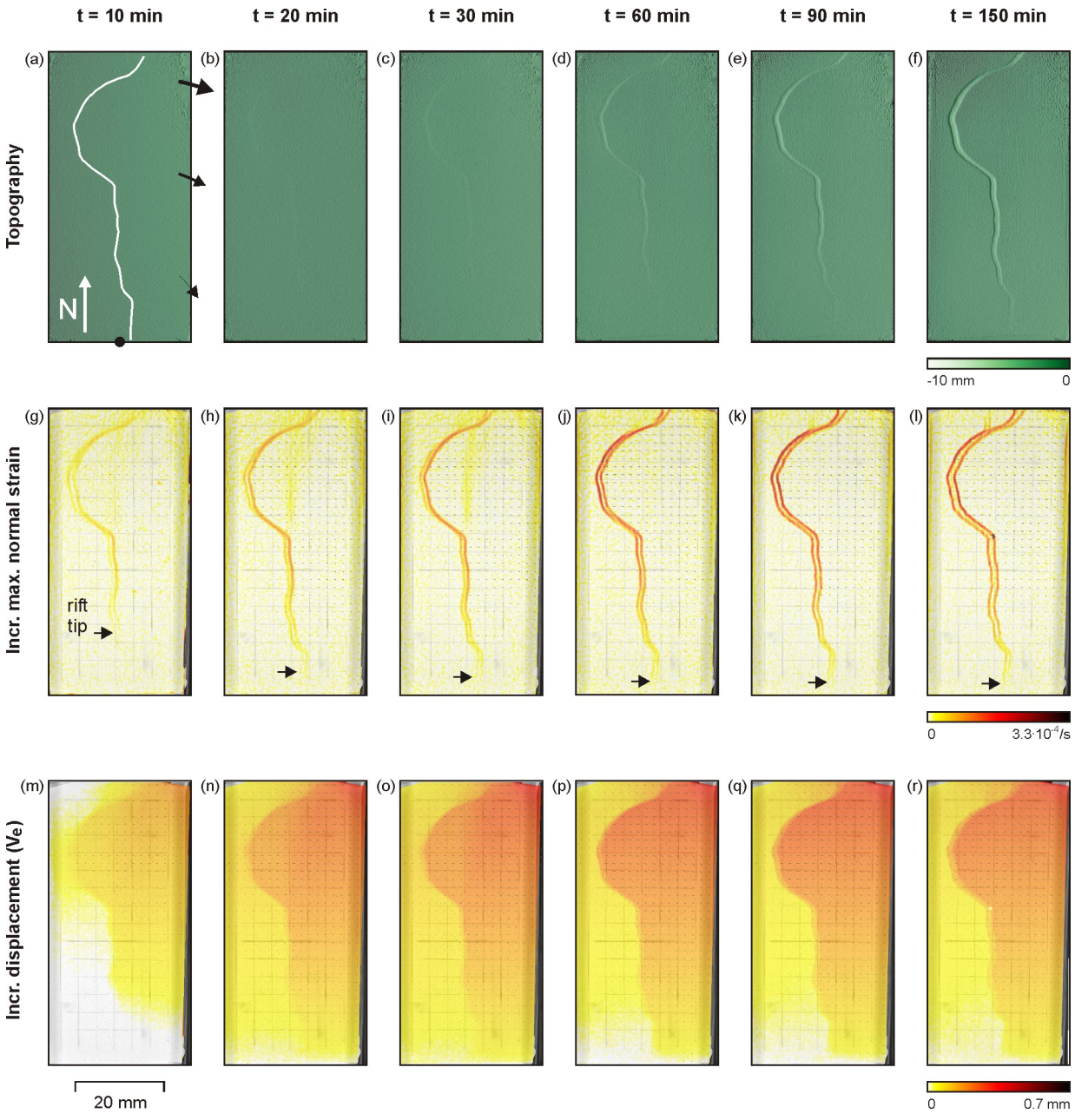

Figure 7: Results of Model E. (a-f) Topography evolution. Initial seed geometry is shown in panel (a). Lighting direction: from the left. (g-l) Incremental maximum normal strain (m-r). Incremental eastward displacement (Ve). Increments for digital image correlation (DIC) analysis: 10 minutes of divergence.

https://doi.org/10.5194/egusphere-2022-1365
Preprint. Discussion started: 2 January 2023

4. Discussion

4.1. Synopsis and comparison to previous modelling studies

In Figure 8 we present a summary overview of our model results, taken at the end of each model run, which forms the basis for a synopsis of model results and comparison to previous modelling studies presented in the following sections.

4.1.1. Rotational rifting

The first important insight from our model results is that the rotational divergence boundary condition leads to an overall northwardly increasing divergence rate that correlates with the most developed rift basins occurring towards the north of the models (Figs. 3-8). This is, however, not a highly surprising insight since the boundary condition dictates that the largest amount of extension occurs away from the rotation axis, and this correlation has been observed in many previous modelling studies involving rotational divergence (e.g. Souriot and Brun 1992; Benes and Scott 1996; Sun et al. 2009; Molnar et al. 2017, 2018; Mondy et al. 2018; Zwaan and Schreurs 2020; Zwaan et al. 2020; Schmid et al. 2022a, b). Still, this first-order agreement with previous works validates our general model results.

A further observation related to rotational divergence in our models is the initial fast rift propagation of extension towards the rotation axis in the south, followed by a deceleration and a slow propagation in the later stages of the model run. This effect was previously reported by Schmid et al. (2022a, b), and is upon closer inspection also visible in the models by Mondy et al. (2018), Maestrelli et al. (2020) and Zwaan et al. (2020). Indeed, this fast propagation of extension is not directly obvious from topography data and requires DIC results to be revealed, highlighting the need for such DIC analysis. It also shows that rift propagation in the models is in fact a much faster process than perhaps previously interpreted from topography data: very early on in the evolution of the models, rifting has started along most of the rift system, establishing the template for its subsequent structural evolution. This is somewhat in contrast to the observations by Zwaan and Schreurs (2020), who had to rely on visual inspection of surface imagery of their models only.

4.1.2. Seed geometry and microplates

Rotational divergence itself would be expected to produce a linear rift system along the axis of the model (e.g. Benes and Scott 1996; Zwaan et al. 2020; Schmid et al. 2022a, b), but the structural inheritance applied in our models forces the model to deviate from this template, generating a range of rift basin arrangements. When comparing the various seed geometries we applied to the final structures produced in the models, the relations are somewhat complex (Fig. 8). In Model A, representing the end member with the dominant rift structures situated farthest to the east, not all seeds are reactivated (Figs. 3, 8a-d). It seems that extension preferentially localized in the north of the model, along the simulated Main Ethiopian and Kenya Rift where the largest degree of extension is applied, before swiftly propagating south along the strike of the model, mostly avoiding the seeds tracing the Western Rift and the eastern margin of the Rovuma plate (Fig. 3g-l). It may very well be that this

https://doi.org/10.5194/egusphere-2022-1365
Preprint. Discussion started: 2 January 2023

orientation of rifting (i.e. near the axis of the system) is ideal in this type of model, so that the seeds that are thus aligned are preferentially activated at the expense of in this case the Western Rift and eastern margin of the Rovuma Plate. Such preferential reactivation of more favourably oriented weaknesses has been observed in various previous modelling studies (e.g. Henza et al. 2010, 2011; Zwaan and Schreurs 2017; Molnar et al. 2019, 2020; Maestrelli et al. 2020; Wang et al. 2021; Zwaan et al. 2021a, 2022a).

However, when these seeds are not fully linked up as in Models B and C, deformation is forced to follow the offset seeds, resulting in a rift pass or overlap configuration (Nelson et al., 1992; Hieronymus, 2004; Kolawole et al., 2021, Figs. 4, 5, 8e-l). The overlapping configuration of these rifts, where one rift becomes dominant over the other along strike, causes the rotation of the central rift pass area (in this case the simulated Victoria plate, Figs. 4m-r, 5m-r, 8h, l). Such rotations of rift pass blocks have been reported in numerous modelling studies (e.g. Oldenburg and Brune, 1975; Katz et al., 2005; Tentler and Acocella, 2010; Zwaan et al., 2016, 2018, 2020; Brune et al., 2017; Molnar et al., 2017, 2018; Glerum et al., 2019; Neuharth et al., 2021). Important in these systems is that both overlapping rifts propagate as the block rotates, which is also seen in our Models B and C (Figs. 4m-r, 5m-r,). In combination with regional-scale rotation, this means that active extension (i.e. rift basins) can propagate both (regionally) towards and (locally) away from the rotation pole, as proposed by Zwaan and Schreurs (2020) (Figs. 4m-r, 5m-r).

Model D (Fig. 8m-p) continues the westward shift in rift localization shown in in Models B and C (Fig. 8e-l). This more westward concentration of rifting is due to the thicker seed tracing the Western Rift, which overrides the tendency of the model to preferentially localize deformation along the central model axis that is shown in Model A (Fig. 8a-e, m-p). A thicker seed represents a more impactful weakness in the system, and such weaknesses naturally attract more deformation, as also observed in previous modelling studies (e.g. Henza et al., 2010, 2011; Wang et al.., 2020; Zwaan et al., 2021a, Osagiede et al., 2021) Even so, the Kenya Rift seed still localized a part of the deformation in the system, creating a Victoria Plate equivalent as in Models B and C, but with the crucial difference that this plate does not rotate counter-clockwise (Figs. 6m-r, 8p). Instead, it merely moves along with the rotation of the eastern domain, albeit at a slower rate due to the presence of the simulated Kenya Rift (Fig. 6m-r). Similar to Model A, the eastern part of the Rovuma plate did not reactivate, very likely due to the same unfavourable arrangement with respect to the overall tectonic set-up (Figs. 6, 8a-d, 8m-p).

Model E is the other end-member model, where the single seed localizes deformation along the Western Rift and Malawi Rift traces (Fig. 8q-t). Even though no seed was present along the Kenya Rift trace, there are some hints of minor early extension localization there, highlighting the model's preference to localize deformation along its central axis (Fig. 6g-j). Nevertheless, the experiment results in a solid eastern domain that rotates eastward in a clockwise orientation (Figs. 6g-l, 8t), without any hint of the Victoria microplate.

https://doi.org/10.5194/egusphere-2022-1365
Preprint. Discussion started: 2 January 2023

4.1.3. Additional observations: intra-rift deformation and oblique rifts

In addition to the large-scale observations described above, some more detailed insights can be gained from our models. Firstly, the DIC analysis shows the initial localization of boundary faults flanking the rift segments, followed by intra-rift deformation along the central axis of the most developed rift basins (Fig. 8d, h, l, p, t). This shift of deformation has been observed on DIC results of previous models (Schmid et al. 2022a, b) as well, and can be explained by the rise of the viscous layer below the rift axis in this type of brittle-viscous models (e.g., Zwaan et al. 2018; 2016; 2020), while the rift boundary faults have accommodated most of their slip at that point in time.

The various orientations of the rift segments provide some final insights. Indeed, there where the rift basins are oriented obliquely with respect to the model axis (and this to the general extension direction), they are much narrower than those rift basins that are parallel to the model axis (Fig. 8b, f, j, n, r). This is a straightforward effect of the local oblique extension direction: the larger the extension obliquity, the more the system moves towards steep strike-slip faulting (e.g. Corti et al. 2007; Zwaan et al. 2016). Here it must be noted that for an exact determination of the extension obliquity, the rotational divergence and the curved displacement traces needs to be taken into account (Fig. 8a, e, i, m, q), but the general orientation of the rifts nwith respect to the model axis provide a first order indication that is sufficiently accurate (see also the Appendix).

A detail that is however not captured in our models are en echelon structures, which are typical of oblique extension models (e.g. Withjack and Jamison 1986; Tron and Brun 1991; Bonini et al. 1997; Keep and McClay 1997; Zwaan et al. 2021a, 2022a). Especially the simulated Western Rift should be expected to contain various sub-basins, as shown by previous models (which do however not incorporate rift propagation, Corti et al. 2007). This is likely due to the large scale of our model set-up, as well as the general brittle-viscous set-up with seeds preventing the development of such details (compare our results with Figs. 5 and 7 in Zwaan and Schreurs 2017). As such, our models are best suited to reveal the large-scale trends in such settings.

https://doi.org/10.5194/egusphere-2022-1365
Preprint. Discussion started: 2 January 2023

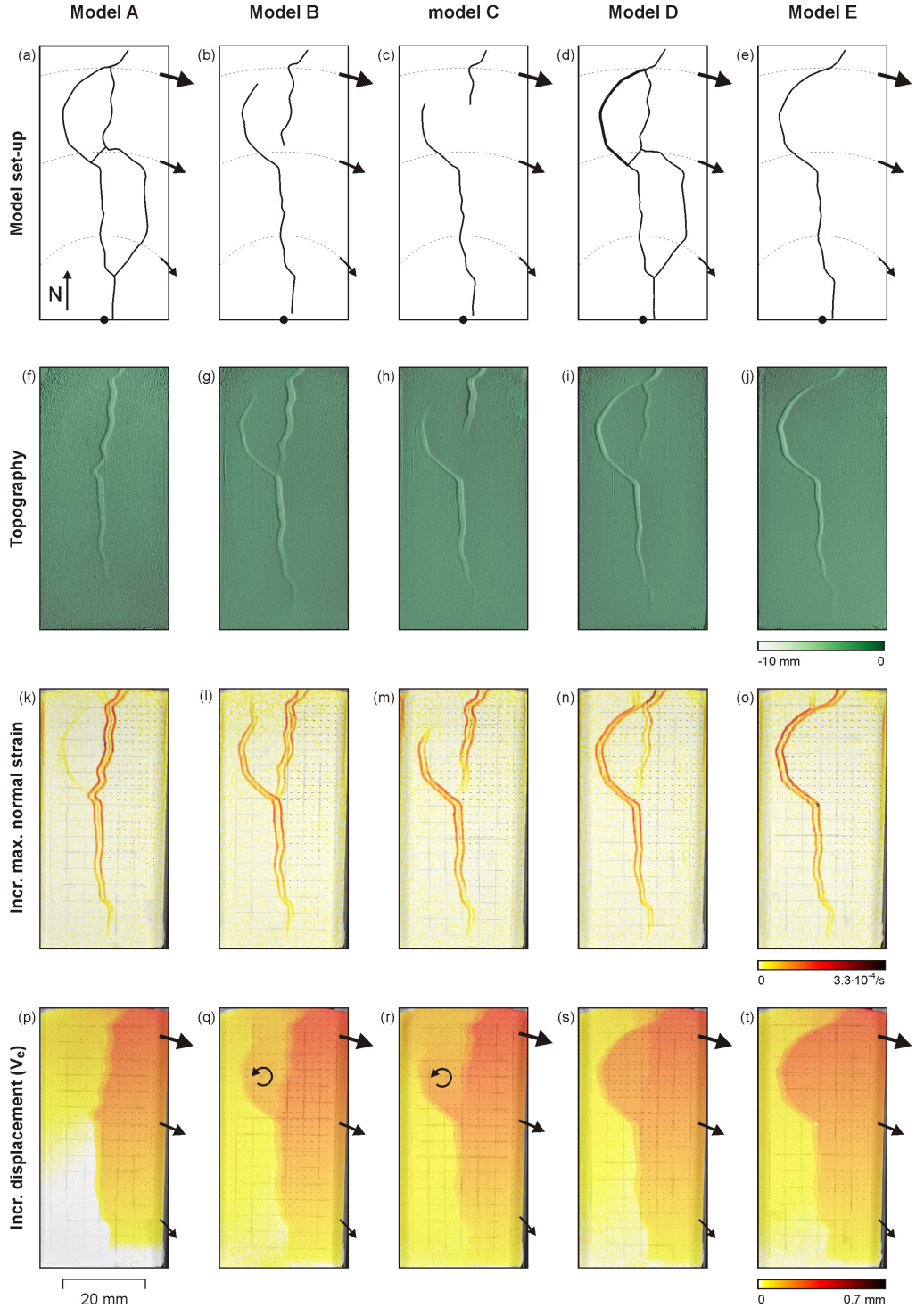

Figure 8: Overview of final stage (t = 150 min) model results from Models A-E. (a-e) General model set-up showing seed geometries and model kinematics. (f-j) Final model topography. (k-o) Incremental maximum normal strain. (p-t) Incremental eastward displacement (Ve). Increments for digital image correlation (DIC) analysis: 10 minutes of divergence.

https://doi.org/10.5194/egusphere-2022-1365
Preprint. Discussion started: 2 January 2023

4.2. General model limitations

Before comparing our model results with the EARS, it is important to point out some limitations of our models. Firstly, as mentioned in section 4.1.3, our models should be used to for the evolution of large-scale tectonic structures. Furthermore, the modelling of rotational divergence on a sphere (as is the case in nature) is done on a flat plane (Zwaan et al. 2020), which may cause some distortions towards the rotation pole and affect the rate of rift propagation in our models (Schmid et al. 2022a, b). Yet these minor effects are not considered to significantly undermine our model results. Some boundary effects occur along the long edges of our model, as shown by the slight rotation of the westernmost domain in our models, but also the impact of these boundary effects are minor on the large-scale evolution of the model. A final limitation is the lack of surface processes (erosion and sedimentation) in our models, which are known to affect rift evolution (e.g. Burov and Cloetingh, 1997; Buiter, 2009; Neuharth et al., 2022). However, the analogue models by Zwaan et al. (2018a) suggest surface processes do not significantly alter the large-scale structures of young continental rift systems, and as such, our model results remain valid on a first-order scale.

4.3. Comparison to the EARS

4.3.1 Rift propagation in the EARS

Of the five rifting models completed for this study, Model C provides the best fit with the EARS (Fig. 9a, b), and we can use the model to discuss the evolution of the natural example. First of all, we can infer a general southward propagation of rift initiation along the whole length of the EARS, as previously proposed by Zwaan and Schreurs, 2020), due to the clockwise rotation of the Somalian Plate (e.g. Saria et al., 2014, Fig. 1a). This southward propagation is in line with data from the EARS showing a southward younging direction of rifting (Chorowicz, 2005; Macgregor, 2015). Importantly, our models also suggest that deformation may already have propagated over large parts of the system during the earlier phases of EARS development, and such a fast southward propagation of EARS structures between ca. 12-5 Ma is inferred by Macgregor (2015) (Fig. 1c-e). It must however be pointed out that the exact initiation of rifting in the various rift basins along the EARS is debated (Zwaan and Schreurs, 2020, Michon et al., 2022, and references therein), and such early extension may have occurred without leaving behind clear field evidence due to the initially limited amount of deformation. A further complication in this context is the magma-rich nature of the EARS, which may cause a strongly localized rift deformation (Buck, 2004, 2006) that is well reproduced by our seeds, and provides dates of rift initiation (e.g. Ayalew et al., 2006; Wolfenden et al., 2005; Michon et al. 2020). However, these records may not always be properly preserved in the sub-aerial conditions of the EARS, which is also the case for any syn-rift sediments.

https://doi.org/10.5194/egusphere-2022-1365
Preprint. Discussion started: 2 January 2023

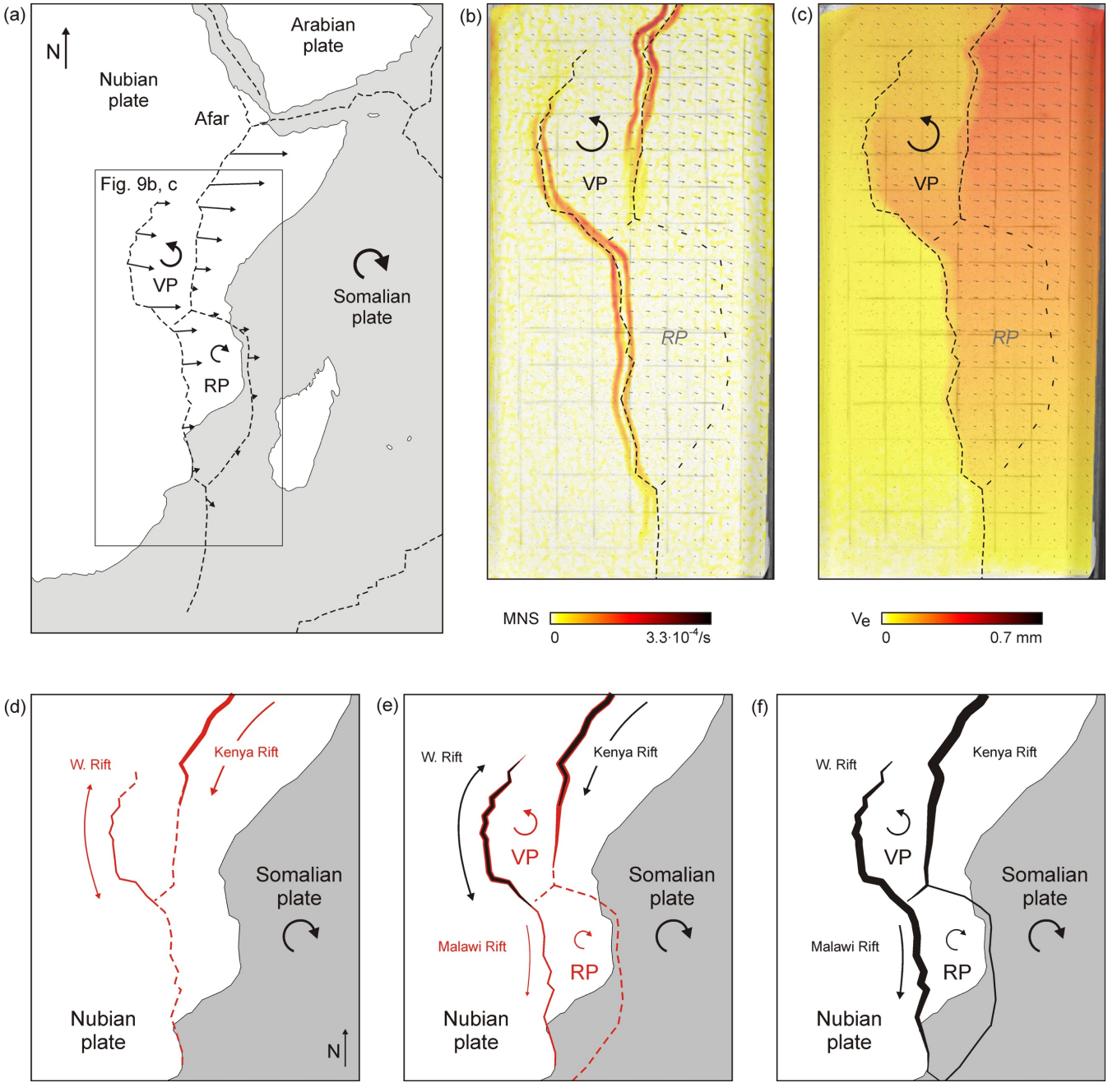

Figure 9: Application of our model results. (a-c) Comparison between the East African Rift System (EARS) and our Model C: (a) tectonic map of the EARS, modified after Saria et al. (2014). (b) Maximum normal strain localization, which follows the general trace of the EARS, and (b) eastward displacement (Ve), which mimics the large-scale plate divergence pattern of the EARS. (d-f) Conceptual evolution of the EARS, involving rapid southward propagation of rift-related extension (red), followed by development of rift basins (black), based on our model results (modified after Zwaan and Scheurs, 2020). VP: Victoria Plate, RP: Rovuma Plate.

https://doi.org/10.5194/egusphere-2022-1365
Preprint. Discussion started: 2 January 2023

All things considered the general southward propagation of the EARS is a simple and convincing model, based on existing field data (Chorowicz, 2005; Macgregor, 2015), GPS data and our experimental results (Fig. 9). Furthermore, our rotational model fits in fact very well with the local orthogonal (E-W) extension model for the Victoria Plate proposed by Glerum et al. (2020); on a local scale extension can be considered more or less orthogonal, the extension gradient only becomes an important factor on a regional scale, affecting the along-strike maturity of the system (Zwaan and Schreurs, 2020, Figs. 8, 9). Finally, as to the influence of the various inherited weaknesses along the EARS, it is clear from our models that the peculiar arrangement of rifts basins in the system is closely related to the distribution of inherited weaknesses, but their precise influence in nature cannot be specified for each case, due to the complexity of the natural case.

4.3.2. Microplates within the EARS

A further key observation in our Model C concerns the evolution of micro plates. The simulated Victoria Plate segregated and started rotating in a counter-clockwise early on during the model run, as a result of the rapid nucleation of the overlapping Western Rift and Kenya Rift model equivalents (Figs. 5m-r, 8l). The same mechanism is indeed clearly active in the EARS, (Glerum et al., 2020, Zwaan and Schreurs, 2020), as also indicated by GPS data (Saria et al., 2014) (Figs. 1a, 9). From our Model C results, we can consider the Victoria Plate to have been present and rotating shortly since the development of the Western and Kenya Rift started around 12 Ma (Fig. 9d), and should have been in full swing by 5 Ma when both rifts were well-established (Fig 9e) (Macgregor, 2015). Similar to our models, we should then also expect the Western Rift to have propagated northward since its early inception, and the Kenya rift should have propagated southward, which is in agreement with observations from the EARS (Macgregor, 2015). During (the early stages of) the Model C run, the southern tip of the simulated Kenya rift also exhibits the diffuse deformation observed in nature (Figs. 1b, 5g-l). We note that in contrast to the Victoria Plate, the Rovuma Plate is not represented in our Model C (or any model for that matter, Fig. 8). However, the Rovuma Plate is situated close to the rotation pole and does involve very minor (<1 mm/yr) motion (Saria et al., 2014, Fig. 1a). Yet a complete model of the EARS will need to incorporate the evolution of the Rovuma plate as well, since it does take up about 30% of the plate divergence in the southern part of the EARS (Fig. 1a). What can be predicted from our models is that the Rovuma Plate, similar to the Victoria plate, was segregated at an early stage in the development of the EARS as extension propagated southward (Fig. 9e).

4.3.3. Intra-rift deformation and oblique rifts in the EARS

Two further details observed in our models are also relevant to our interpretation of the EARS. The first is the localization of intra-rift extension along the central axis of the most evolved rift basins (Fig. 8c, g, k, o, s). Such localization is also observed in the MER, which represent the most evolved part of the EARS, except for the Afar triangle (Fig. 1a). Here so-called magmatic segments belonging to the Wonji Fault Belt are situated along the rift axis, and are found to accommodate a significant portion

https://doi.org/10.5194/egusphere-2022-1365
Preprint. Discussion started: 2 January 2023

of the total extension in the system (e.g. Ebinger, 2005; Pizzi et al., 2006; Ebinger et al., 2008). The second observation concerns the impact of rift orientation on rift structures. Although our models do not provide detailed insights into fault structures, the general oblique / strike-slip nature of the obliquely oriented rift segments such as the Rukwa Rift is clearly recognized (Figs. 8d-t, 9b).

5. Conclusion

In this study we present a new series of rotational rifting models specifically tailored to explore the dynamic evolution of the East African Rift System (EARS) within the broader rotational rifting framework. Our model results lead us to the following conclusions:

- Rotational rifting leads to rift propagation in all our model runs. Yet we need to distinguish between the propagation of rift-related deformation, which can move very rapidly towards the rotation axis, and the surface expression of this rapidly propagating deformation, which can significantly lag behind. We propose that such rapid propagation may have taken place in the EARS as well.
- Various structural weakness arrangement in our models lead to a variety of different structures. It is clear that laterally overlapping weaknesses are required for localizing parallel rift basins to create rift pass structures, possibly leading to the segregation of micro-plates. These plates can start rotating if the rift basins on both sides are sufficiently developed and become laterally dominant, as is the case for the Victoria Plate in the EARS, and likely also for the Rovuma Plate.
- Additional model observations involve the development of early pairs of rift-bounding faults flanking the rift basins, followed by the localization of deformation along the axes of the most developed parts of the rift system. Such a shift of deformation towards the centre of the rift has been observed along the MER, (along the Main Ethiopian Rift), and is associated with incipient continental break-up.
- Finally, we observe how the orientation of rift segments with respect to the regional (rotational) plate divergence affect deformation along these segments. Compared to rift segments that are oriented perpendicular to the plate divergence direction, obliquely oriented rift segments are less wide and show a component of strike-slip deformation (i.e. oblique extension.
- Overall, we find that our model results provide a good fit with the large-scale features of the EARS, and provide constraints on the timing of general rift development, and the segregation and rotation of the Victoria plate within the broader rotational rifting framework of the EARS.

https://doi.org/10.5194/egusphere-2022-1365
Preprint. Discussion started: 2 January 2023

Author contribution

FZ designed and carried out the experiments, analysed the experimental results, and wrote the original draft of this paper. GS secured funding, took care of project administration and critically reviewed the original draft.

Competing interests

The authors declare that they have no competing interests.

Data availability

Extensive overviews and videos of our modelling results are provided in the form of a GFZ data publication (Zwaan et al. 2023). NB: this data publication is in preparation but the files can already be accessed in this Dropbox folder: https://www.dropbox.com/sh/6k34psul6cij4dh/AABpt-cnM1OyIEdolfTszmmya?dl=0

Acknowledgements

We thank Timothy Schmid from the University of Bern Tectonic Modelling group for helping with the DIC analysis, and to Florian Ott and Kirsten Elger from GFZ Potsdam for helping us prepare the GFZ data publication containing the supplementary data of this paper (Zwaan et al. 2023). This project was funded by the Swiss National Science Foundation (SNSF) through grant 200021-178731 "4D Analogue modelling of oblique rifts and obliquely rifted margins" (https://data.snf.ch/grants/grant/178731). The SNSF also covered the Open Access publication costs.

Appendix

The five models presented in the main text all have a minor error in that the location of the rotation axis is in fact somewhat too far to the west (Fig. A1). Although this error does somewhat modify the relative direction of plate divergence along the seeds (Fig. A1a, e), the final result in both Model A, and Model F with the correct rotation axis location are very similar (Fig. A1. Hence, we conclude that the results from our Models A-E as presented in this paper remain valid.

https://doi.org/10.5194/egusphere-2022-1365
Preprint. Discussion started: 2 January 2023

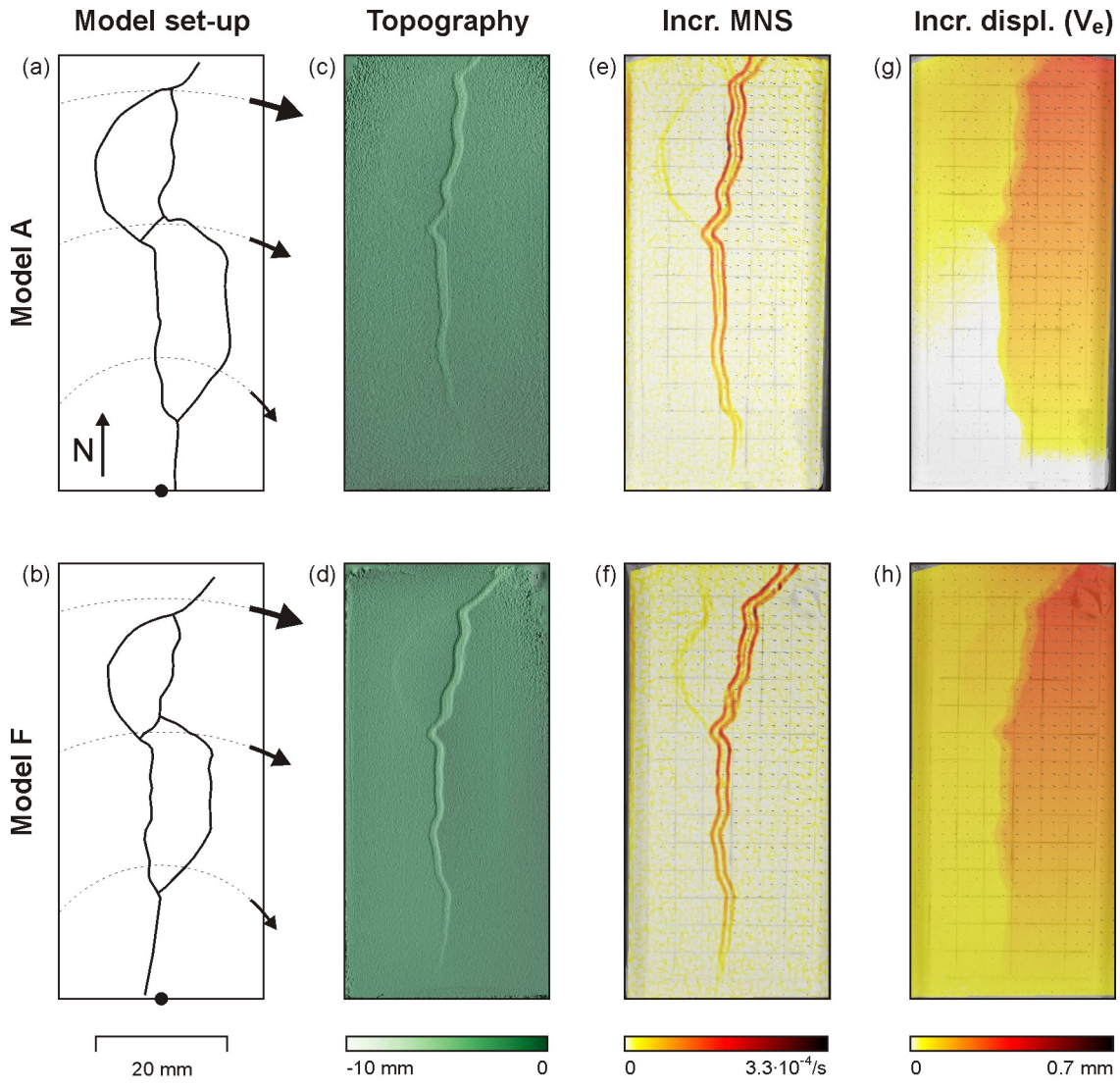

Figure A1: Comparison of final stage (t = 150 min) model results from Models A and F. (a-b) General model set-up showing seed geometries and model kinematics. (c-d) Final model topography. (e-f) Incremental maximum normal strain (MNS). (g-h) Incremental eastward displacement (V_e). Increments for digital image correlation (DIC) analysis: 10 minutes of divergence.

https://doi.org/10.5194/egusphere-2022-1365
Preprint. Discussion started: 2 January 2023

References

Adam, J., Urai, J. L., Wieneke, B., Oncken, O., Pfeiffer, K., Kukowski, N., and Lohrmann, J.: Shear localisation and strain distribution during tectonic faulting — new insights from granular-flow experiments and high-resolution optical image correlation techniques, J. Struct. Geol., 27, 283–301, https://doi.org/10.1016/j.jsg.2004.08.008, 2005.

Ayalew, D., Ebinger, C., Bourdon, E., Wolfenden, E., Yirgu, G., and Grassineau, N.: Temporal compositional variation of syn-rift rhyolites along the western margin of the southern Red Sea and northern Main Ethiopian Rift, Geol. Soc. Spec. Publ., 259, 121-130, https://doi.org/10.1144/GSL.SP.2006.259.01.10, 2006.

Benes, V., and Scott, S. D.: Oblique rifting in the Havre Trough and its propagation into the continental margin of New Zealand: Comparison with analogue experiments, Mar. Geophys. Res., 18, 189-201, https://doi.org/10.1007/BF00286077, 1996.

Bonini, M., Souriot, T., Boccaletti, M., and Brun, J. -P.: Successive orthogonal and oblique extension episodes in a rift zone: Laboratory experiments with application to the Ethiopian Rift, Tectonics, 16, 347-362, https://doi.org/10.1029/96TC03935, 1997.

Boutelier, D., Schrank, C., and Regenauer-Lieb, K.: 2-D finite displacements and finite strain from PIV analysis of plane-strain tectonic analogue models, Solid Earth, 10, 1123-1139, https://doi.org/10.5194/se-10-1123-2019, 2019.

Brun, J. -P.: Narrow rifts versus wide rifts: inferences for the mechanics of rifting from laboratory experiments, Phil. T. R. Soc. A, 357, 695-712, https://doi.org/10.1098/rsta.1999.0349, 1999.

Brune, S., Corti, G., and Ranalli, G.: Controls of inherited lithospheric heterogeneity on rift linkage: Numerical and analogue models of interaction between the Kenyan and Ethiopian rifts across the Turkana depression, Tectonics, 36, 1767–1786, https://doi.org/10.1002/2017TC004739, 2017.

Buck, R. W.: The role of magma in the development of the Afro-Arabian Rift System, Geol Soc. Spec. Publ., 259, 43-54, https://doi.org/10.1144/GSL.SP.2006.259.01.05, 2004.

Buck, R. W.: Consequences of Asthenospheric Variability on Continental Rifting, in: Rheology and Deformation of the Lithosphere at Continental Margins, edited by: Karner, G. D., Taylor, B., Driscoll, N. W., and Kohlstedt, D. L., Columbia University Press, New York, USA, 1-30. https://doi.org/10.7312/karn12738-002, 2004.

https://doi.org/10.5194/egusphere-2022-1365
Preprint. Discussion started: 2 January 2023

Buiter, S. J. H., Pfiffner, O. A., and Beaumont, C.: Inversion of extensional sedimentary basins: A numerical evaluation of the localisation of shortening, Earth Planet. Sci. Lett., 288, 492–504., https://doi.org/10.1016/j.epsl.2009.10.011, 2009.

Burov, E., and Cloetingh, S.: Erosion and rift dynamics: new thermomechanical aspects of post-rift evolution of extensional basins, Earth Planet. Sc. Lett., 150, 7-26, https://doi.org/10.1016/S0012-821X(97)00069-1, 1997.

Byerlee, J.: Friction of Rocks, Pure Appl. Geophys., 116, 615-626, https://doi.org/10.1007/BF00876528, 1978.

Carlo AG (Carlo Bernasconi AG, Switzerland, company website): www.carloag.ch, last access: 29 Nov 2022.

Chorowicz, J.: The East African rift system, J. Afr. Earth. Sci., 43, 379-410, https://doi.org/10.1016/j.jafrearsci.2005.07.019, 2005.

Corti, G: Evolution and characteristics of continental rifting: Analog modeling-inspired view and comparison with examples from the East African Rift System, Tectonophysics, 522-523, 1-33, https://doi.org/10.1016/j.tecto.2011.06.010, 2012

Corti, G., Van Wijk, J., Cloetingh, S., and Morley, C. K.: Tectonic inheritance and continental rift architecture: Numerical and analogue models of the East African Rift system, Tectonics 26, TC6006, https://doi.org/10.1029/2006TC002086, 2007.

Souriot, T., and Brun, J. -P.: Faulting and block rotation in the Afar triangle, East Africa: The Danakil "crank-arm" model, Geology, 20, 911–914. https://doi.org/10.1130/0091-7613(1992)020<0911:FABRIT>2.3.CO;2, 1992.

Delvaux, D., Kervyn, F., Macheyeki, A., and Temu, E: Geodynamic significance of the TRM segment in the East African Rift (W-Tanzania): Active tectonics and paleostress in the Ufipa plateau and Rukwa basin, J. Struct. Geol., 37, 161–180, https://doi.org/10.1016/j.jsg.2012.01.008, 2012.

Ebinger, C. J.: Tectonic development of the western branch of the East African rift system, GSA Bull., 101, 885-903, https://doi.org/10.1130/0016-7606(1989)101<0885:TDOTWB>2.3.CO;2, 1989.

Ebinger, C. J.: Contental break-up: The East African perspective, Astronomy and Geophysics, 46, 2.16-2.21, https://doi.org/10.1111/j.1468-4004.2005.46216.x, 2005.

Ebinger, C. J., Keir, D., Ayele, A., Calais, E., Wrigth, T. J., Belachew, M., Hammond, J. O. S., Campbell, E., and Buck, R. W.: Capturing magma intrusion and faulting processes during continental rupture: seismicity of the Dabbahu (Afar) rift, Geophys. J. Int., 174, 1138–1152, https://doi.org/10.1111/j.1365-246X.2008.03877.x, 2008.

Glerum, A., Brune, S., Stamps, D. S., and Strecker, M. R.: Victoria continental microplate dynamics controlled by the lithospheric strength distribution of the East African Rift, Nat. Commun., 11, 2881, https://doi.org/10.1038/s41467-020-16176-x, 2020.

Henza, A. A., Withjack, M. O., and Schlische, R. W.: Normal-fault development during two phases of non-coaxial extension: An experimental study, J. Struct. Geol., 32, 1656-1667, https://doi.org/10.1016/j.jsg.2009.07.007, 2010.

Henza, A. A., Withjack, M. O., and Schlische, R. W.: How do the properties of a pre-existing normal-fault population influence fault development during a subsequent phase of extension?, J. Struct. Geol., 33, 1312–1324, https://doi.org/10.1016/j.jsg.2011.06.010, 2011.

Hieronymus, C. F.: Control on seafloor spreading geometries by stress- and strain-induced lithospheric weakening, Earth Planet. Sc. Lett., 222, 177-189, https://doi.org/10.1016/j.epsl.2004.02.022, 2004.

Hubbert, M. K.: Theory of scaled models as applied to the study of geological structures, Geol. Soc. Am. Bull., 48, 1459-1520, https://doi.org/10.1130/GSAB-48-1459, 1937.

Katz, R. F., Ragnarsson, R., and Bodenschatz, E.: Tectonic microplates in a wax model of sea-floor spreading, New J. Phys., 7, 37, https://doi.org/10.1088/1367-2630/7/1/037, 2005.

Keep, M., and McClay, K. R.: Analogue modelling of multiphase rift systems, Tectonophysics, 273, 239, https://doi.org/10.1016/S0040-1951(96)00272-7, 1997.

Kolawole, F., Firkins, M. C., Al Wahaibi, T. S., Atekwana, E. A., and Soreghan, M. J.: Rift interaction zones and the stages of rift linkage in active segmented continental rift systems, Basin Res., 33, 2984– 3020, https://doi.org/10.1111/bre.12592, 2021.

Macgregor, D.: History of the development of the East African Rift System: A series of interpreted maps through time, J. Afr. Earth. Sc., 101, 232-252, https://doi.org/10.1016/j.jafrearsci.2014.09.016, 2015.

https://doi.org/10.5194/egusphere-2022-1365
Preprint. Discussion started: 2 January 2023

Maestrelli, D., Montanari, D., Corti, G., Del Ventisette, C., Moratti, G., and Bonini, M.: Exploring the Interactions Between Rift Propagation and Inherited Crustal Fabrics Through Experimental Modeling, Tectonics, 39, e2020TC006211, https://doi.org/10.1029/2020TC006211, 2020.

Michon, L., Famin, V, and Quicelleur, X.: Evolution of the East African Rift System from trap-scale to plate-scale rifting, Earth. Sc. Rev., 231, 104089, https://doi.org/10.1016/j.earscirev.2022.104089, 2022.

Molnar, N. E., Cruden, A. R., and Betts, P. G.: Interactions between propagating rotational rifts and linear rheological heterogeneities: Insights from three-dimensional laboratory experiments, Tectonics, 36, 420–443, https://doi.org/10.1002/2016TC004447, 2017.

Molnar, N. E., Cruden, A. R., and Betts, P. G.: Unzipping continents and the birth of microcontinent, Geology, 46, 451-454, https://doi.org/10.1130/G40021.1, 2018.

Molnar, N. E., Cruden, A. R., and Betts, P. G.: Interactions between propagating rifts and linear weaknesses in the lower crust, Geosphere, 15, 1617-1640, https://doi.org/10.1130/GES02119.1, 2019.

Molnar, N. E., Cruden, A. R., and Betts, P. G.: The role of inherited crustal and lithospheric architecture during the evolution of the Red Sea: Insights from three dimensional analogue experiments, Earth. Planet. Sc. Lett., 544, 116377, https://doi.org/10.1016/j.epsl.2020.116377, 2020.

Mondy, L. S., Rey, P. f., Ducleaux, G., and Moresi, L.: The role of asthenospheric flow during rift propagation and breakup, Geology, 46, 103-106, https://doi.org/10.1130/G39674.1, 2018.

Morley, C.K., Ngenoh, D.K., and Ego., J.K.: Introduction to the East African Rift System, in: Geoscience of Rift Systems—Evolution of East Africa, edited by Morley C.K., AAPG Studies in Geology, 44, pp. 1–18, https://doi.org/10.1306/St44623C1, 1999.

Morley, C. K.: Stress re-orientation along zones of weak fabrics in rifts: An explanation for pure extension in 'oblique' rift segments?, Earth Planet Sci. Lett., 297, 667-673, https://doi.org/10.1016/j.epsl.2010.07.022, 2010.

Mulugeta, G.: Squeeze box in a centrifuge. Tectonophysics, 148, 323-335, https://doi.org/10.1016/0040-1951(88)90139-4, 1988.

https://doi.org/10.5194/egusphere-2022-1365
Preprint. Discussion started: 2 January 2023

Nelson, R. A., Patton, T. L., and Morley, C. K.: Rift-Segment Interaction and Its Relation to Hydrocarbon Exploration in Continental Rift Systems, AAPG Bull., 76, 1153-1169, https://doi.org/10.1306/BDFF898E-1718-11D7-8645000102C1865D, 1992.

Neuharth, D., Brune, S., Glerum, A., Heine, C., and Welford, J. K.: Formation of continental microplates through rift linkage: Numerical modeling and its application to the Flemish Cap and Sao Paulo Plateau, Geochem., Geophys,, Geosys., 22, e2020GC009615, https://doi.org/10.1029/2020GC009615, 2021.

Neuharth, D., Brune, S., Wrona, T., Glerum, A., Braun, J., and Yuan, X.: Evolution of rift systems and their fault networks in response to surface processes, Tectonics, 41, e2021TC007166, https://doi.org/10.1029/2021TC007166, 2022.

Lezzar, K. E., Tiercelin, J. -J., Le Turdu, C., Cohen, A. S., Reynolds, D., J., Le Gall, B., and Scholz, C. A.: Control of Normal Fault Interaction on the Distribution of Major Neogene Sedimentary Depocenters, Lake Tanganyika, East African Rift, AAPG Bull., 86, 1027–1059, https://doi.org/10.1306/61EEDC1A-173E-11D7-8645000102C1865D, 2002.

Oldenburg, D. W., and Brune, J. N.: An explanation for the orthogonality of ocean ridges and transform faults, J. Geophys. Res., 80, 2575– 2585, https://doi.org/10.1029/JB080i017p02575, 1975.

Osagiede, E. E., Rosenau, M., Rotevatn, A., Gawthorpe, R., Jackson, C. A-L., and Rudolf, M.: Influence of zones of pre-existing crustal weakness on strain localization and partitioning during rifting: Insights from analog modeling using high-resolution 3D digital image correlation, Tectonics, 40, e2021TC006970, https://doi.org/10.1029/2021TC006970, 2021.

Panien, M., Schreurs, G, Pfiffner, A.: Mechanical behaviour of granular materials used in analogue modelling: insights from grain characterisation, ring-shear tests and analogue experiments, J. Struct. Geol., 28, 1710-1724, https://doi.org/10.1016/j.jsg.2006.05.004, 2006.

Pizzi, A., Coltorti, M., Abebe, B., Disperati, L., Sacchi, G., and Salvini, R.: The Wonji fault belt (Main Ethiopian Rift): structural and geomorphological constraints and GPS monitoring, Geol. Soc. Spec. Publ., 259, 191-207, https://doi.org/10.1144/GSL.SP.2006.259.01.16, 2006.

Ramberg, H.: Gravity, Deformation and the Earth's Crust, Academic Press, London, 1981.

Ring, U.: The East African Rift System, Austrian J. Earth. Sc., 107, 132-146, http://earthjay.com/earthquakes/20180308_malawi/ring_2014_east_africa_rift.pdf, 2014.

https://doi.org/10.5194/egusphere-2022-1365
Preprint. Discussion started: 2 January 2023

Rudolf, M., Boutelier, D., Rosenau, M., Schreurs, G., and Oncken, O.: Rheological benchmark of silicone oils used for analog modeling of short- and long-term lithospheric deformation, Tectonophysics 684, 12-22, http://dx.doi.org/10.1016/j.tecto.2015.11.028, 2016.

Saria, E., Calais, E., Stamps, D. S., Delvaux, D., and Hartnady, C. J. H.: Present-day kinematics of the East African Rift, J. Geophys. Res.-Sol. Ea., 119, 3584-3600, https://doi.org/10.1002/2013JB010901, 2014.

Scott, D. L., Rosendahl., B. R., Burgess, C. F., and Sander, S.: Comments on "variable extension in Lake Tanganyika" by C.K. Morley, Tecotnics, 8, 647-650, https://doi.org/10.1029/TC008i003p00647, 1989.

Schmid, T., Schreurs, G., Warsitzka, M., Rosenau, M.: Effect of sieving height on density and friction of brittle analogue material: Ring-shear test data of quarz sand used for analogue experiments in the Tectonic Modelling Lab of the University of Bern, GFZ Data Services, https://doi.org/10.5880/fidgeo.2020.006, 2020.

Schmid, T. C., Schreurs, G., Adam, J.: Characteristics of continental rifting in rotational systems: New findings from spatiotemporal high resolution quantified crustal scale analogue models, Tectonophysics, 822, 229174, https://doi.org/10.1016/j.tecto.2021.229174, 2022a.

Schmid, T. C., Schreurs, G., and Adam, J.: Rotational extension promotes coeval upper crustal brittle faulting and deep-seated rift-axis parallel flow: Dynamic coupling processes inferred from analog model experiments, J. Geophys. Res. Solid Earth, 127, e2022JB024434, https://doi.org/10.1029/2022JB024434, 2022b.

Stamps, D. S., Flesch, L.M., Calais, E., and Ghosh. A.: Current kine- matics and dynamics of Africa and the East African Rift System, J. Geo- phys. Res. Solid Earth, 119, 5161–5186, doi:10.1002/2013JB010717.

Stamps, D. S., Kreemer, C., Fernandes, R., Rajaonarison, T. A., and Rombolamanana, G.: Redefining East African Rift System kinematics, Geology, 49, 150-155, https://doi.org/10.1130/G47985.1, 2021.

Sun., Z., Zhong, Z., Keep, M., Zhou, D., Cai, D., Li, X., Wu, S., and Jiang, J.: 3D analogue modelling of the South China Sea: A discussion on breakup pattern, J. Asian Earth Sci., 34, 544-556, https://doi.org/10.1016/j.jseaes.2008.09.002, 2009.

Tentler, T, and Acocella, V.: How does the initial configuration of oceanic ridge segments affect their interaction? Insights from analogue models, J. Geophys. Res., 115, B01401, https://doi.org/10.1029/2008JB006269, 2010.

https://doi.org/10.5194/egusphere-2022-1365
Preprint. Discussion started: 2 January 2023

Tron, V., and Brun, J.-P.: Experiments on oblique rifting in brittle-ductile systems, Tectonophysics, 188, 71–88, https://doi.org/10.1016/0040-1951(91)90315-J, 1991.

Wang, L., Maestrelli, D., Corti, G., Zou, Y., and Shen, C.: Normal fault reactivation during multiphase extension: Analogue models and application to the Turkana Depression, East Africa, Tectonophysics, 811, https://doi.org/10.1016/j.tecto.2021.228870, 2021.

Weijermars, R., and Schmeling, H.: Scaling of Newtonian and non-Newtonian fluid dynamics without inertia for quantitative modelling of rock flow due to gravity (including the concept of rheological similarity), Phys. Earth Planet. In., 43, 316-330, https://doi.org/10.1016/0031-9201(86)90021-X, 1986.

Wheeler, W. H., and Karson, J. A.: Extension and subsidence adjacent to a "weak" continental transform: An example from the Rukwa rift, East Africa, Geolog, 22, 625–628, https://doi.org/10.1130/0091-7613(1994)022<0625:EASATA>2.3.CO;2, 1994.

Withjack, M. O. and Jamison, W. R.: Deformation produced by oblique rifting, Tectonophysics, 126, 99–124, https://doi.org/10.1016/0040-1951(86)90222-2, 1986.

Wolfenden, E., Ebinger, C., Yirgu, G., Renne, P. R., and Kelley, S. P.: Evolution of a volcanic rifted margin: Southern Red Sea, Ethiopia, GSA Bull., 117, 846-864, https://doi.org/10.1130/B25516.1, 2005

Zwaan, F., and Schreurs, G.: How oblique extension and structural inheritance influence rift segment interaction: Insights from 4D analog models, Interpretation, 5, SD119-SD138, https://doi.org/10.1190/INT-2016-0063.1, 2017.

Zwaan, F. and Schreurs, G.: Rift segment interaction in orthogonal and rotational extension experiments: Implications for the large-scale development of rift systems, J. Struct. Geol., 140, 104119. https://doi.org/10.1016/j.jsg.2020.104119, 2020.

Zwaan, F, and Schreurs, G.: Time-lapse imagery, digital image correlation (DIC) and topographic analysis of laboratory experiments simulating the evolution of the East African Rift System, GFZ Data Services, 2023.
NB: this data publication is in preparation but the files can already be accessed in this Dropbox folder:
https://www.dropbox.com/sh/6k34psul6cij4dh/AABpt-cnM1OyIEdolfTszmmya?dl=0

https://doi.org/10.5194/egusphere-2022-1365
Preprint. Discussion started: 2 January 2023

Zwaan, F., Schreurs, G. and Adam, J.: Effects of sedimentation on rift segment evolution and rift interaction in orthogonal and oblique extensional settings: Insights from analogue models analysed with 4D X-ray computed tomography and digital volume correlation techniques, Global and Planet. Change, 171, 110-133, https://doi.org/10.1016/j.gloplacha.2017.11.002, 2018a.

Zwaan, F., Schreurs, G., Gentzmann, R., Warsitzka, M. and Rosenau, M.: Ring-shear test data of quartz sand from the Tectonic Modelling Lab of the University of Bern (CH), V. 1. GFZ Data Services, http://doi.org/10.5880/fidgeo.2018.028, 2018b.

Zwaan, F., Schreurs, G., Ritter, M., Santimano, T. and Rosenau, M.: Rheology of PDMS-corundum sand mixtures from the Tectonic Modelling Lab of the University of Bern (CH), V. 1. GFZ Data Services, http://doi.org/10.5880/fidgeo.2018.023, 2018c.

Zwaan, F., Schreurs, G., and Buiter, S. J. H.: A systematic comparison of experimental set-ups for modelling extensional tectonics, Solid Earth, 10, 1063-1097, https://doi.org/10.5194/se-10-1063-2019, 2019.

Zwaan, F., Schreurs, G., Naliboff, J., and Buiter, S.J.H.: Insights into the effects of oblique extension on continental rift interaction from 3D analogue and numerical models, Tectonophysics, 693, 239-260, https://doi.org/10.1016/j.tecto.2016.02.036, 2016.

Zwaan, F., Schreurs, G., and Rosenau, M.: Rift propagation in rotational versus orthogonal extension: Insights from 4D analogue models, J. Struct. Geol., 135, 103946, https://doi.org/10.1016/j.jsg.2019.103946, 2020.

Zwaan, F., Chenin, P., Erratt, D., Manatschal, G., and Scheurs, G.: Complex rift patterns, a result of interacting crustal and mantle weaknesses, or multiphase rifting? Insights from analogue models, Solid Earth, 12, 1473-1495, https://doi.org/10.5194/se-12-1473-2021, 2021.

Zwaan, F., Chenin, P., Erratt, D., Manatschal, G., and Scheurs, G.: Competition between 3D structural inheritance and kinematics during rifting: insights from analogue models, Basin Res., 1–31. https://doi.org/10.1111/bre.12642, 2022.